HHS Public Access

Author manuscript

Neuron. Author manuscript; available in PMC 2020 August 07.

Published in final edited form as:

Neuron. 2019 August 07; 103(3): 489–505.e7. doi:10.1016/j.neuron.2019.05.029.

A discrete dorsal raphe to basal amygdala 5-HT circuit calibrates aversive memory

Ayesha Sengupta[1,*], **Andrew Holmes**[1,2,*]

[1]Laboratory of Behavioral and Genomic Neuroscience, NIAAA, NIH, Rockville, MD, USA

[2]Lead Contact

Summary

Despite a wealth of clinical and preclinical data implicating the serotonin (5-HT) system in fear-related affective disorders, a precise definition of this neuromodulator's role in fear remains elusive. Using convergent anatomical and functional approaches, we interrogate the contribution to fear of basal amygdala (BA) 5-HT inputs from the dorsal raphe nucleus (DRN). We show the DRN→BA 5-HT pathway is engaged during fear memory formation and retrieval, and activity of these projections facilitates fear and impairs extinction. The DRN→BA 5-HT pathway amplifies fear-associated BA neuronal firing, and theta power and phase-locking. Although fear recruits 5-HT/VGluT3 co-expressing DRN neurons, the fear-potentiatinginfluence of the DRN→BA 5-HT pathway requires signalling at BA 5-HT1A/2A receptors. Input/output mapping illustrates how the DRN→BA 5-HT pathway is anatomically distinct and connected with other brain regions that mediate fear. These findings reveal how a discrete 5-HT circuit orchestrates a broader neural network to calibrate aversive memory.

Graphical Abstract

Sengupta and Holmes use *in vivo* imaging, optogenetic, electrophysiological, and histological approaches to investigate the circuit-specific role of the DRN→BA 5-HT pathway in fear learning. They show this pathway is uniquely positioned, functionally and anatomically, to shape fear memory.

[*]Correspondence: ayesha.sengupta@nih.gov, holmesan@mail.nih.gov.

Author Contributions

Conceptualisation, A.S., A.H.; Methodology, A.S., A.H.; Formal Analysis, A.S., A.H.; Investigation, A.S.; Resources, A.H.; Writing—Original Draft, A.S., A.H.; Visualisation, A.S.; Funding Acquisition, A.H.

Declaration of Interests

The authors declare no competing interests.

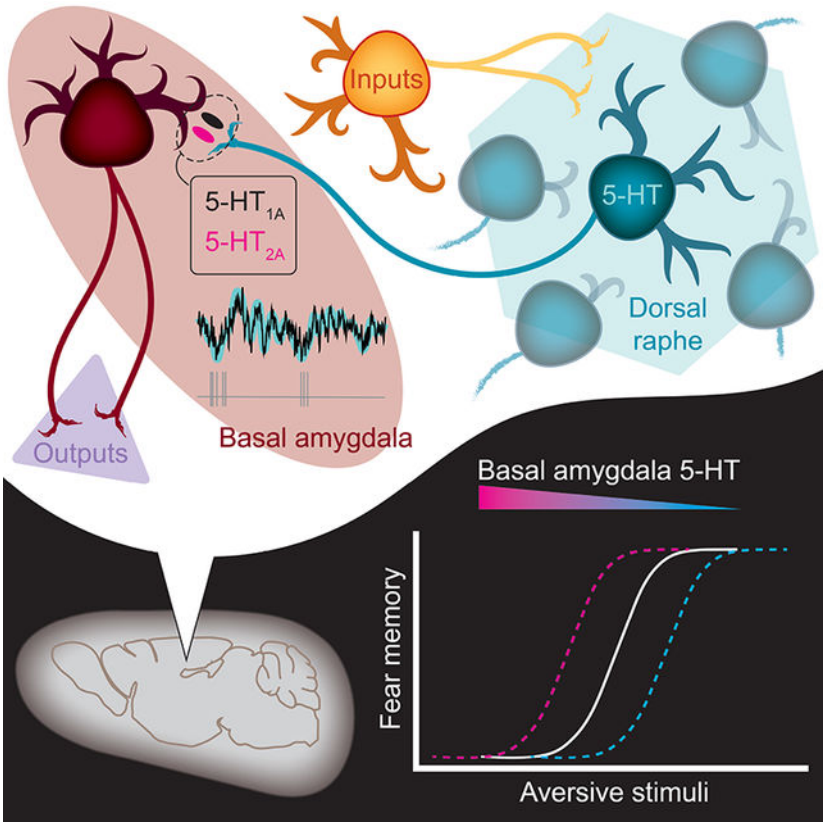

Introduction

Learning about danger and adjusting behaviour accordingly is crucial for survival, but when fear becomes excessive to the threat posed, it can lead to affective disorders (Parsons and Ressler, 2013). Though recent years have seen advancements in elucidating the neural substrates of conditioned threat (‘fear’) (LeDoux, 2014), these mechanisms remain incompletely understood (Bocchio et al., 2017; Tovote et al., 2015).

Converging evidence implicates the serotonin (5-hydroxytryptamine, 5-HT) system in fear. 5-HT-targeting drugs (e.g. 5-HT transporter (5-HTT) inhibitors) are first-line treatments for affective disorders (Holmes, 2008; Nemeroff and Owens, 2002). In animal models, genetic manipulations of 5-HT-related genes alter fear and anxiety-related phenotypes (Caspi et al., 2010; Holmes et al., 2003; Line et al., 2011, 2014; Nonkes et al., 2012; Weisstaub et al., 2006; Zhuang et al., 1999) and suggest disturbances in 5-HT transmission in brain regions mediating fear, such as the amygdala, underly these behavioural effects (Holmes, 2008; Homberg and Lesch, 2011).

5-HT neurons arising from the dorsal raphe nucleus (DRN) densely innervate the amygdala, primarily the basal nucleus (BA) (Sengupta et al., 2017; Steinbusch, 1981), a key node within the broader fear circuitry (Pape and Pare, 2010). BA neurons encode fear and extinction, and loss-of-function BA manipulations impair fear acquisition and/or expression (Akirav et al., 2006; Anglada-Figueroa and Quirk, 2005; Herry et al., 2008; Namburi et al.,

2015; Sierra-Mercado et al., 2011). Yet it is unclear how BA neurons are modulated by 5-HT to impact fear (Bocchio et al., 2015, 2016; Jiang et al., 2009; Rainnie, 1999; Sengupta et al., 2017); fear-related effects of systemic and intra-amygdala administration of 5-HT-acting compounds have been inconsistent (Baratta et al., 2016; Cornélio and Nunes-de-Souza, 2007; Inoue et al., 2004; Izumi et al., 2012; Johnson et al., 2015; Li et al., 2006; Liang, 1999; Macedo et al., 2007; Matsuzaki et al., 2011).

Difficulty delineating the contribution of 5-HT to fear reflects the complexity of 5-HT signalling, which occurs via at least 14 5-HT receptor (5-HT-R) subtypes, and a paucity of methods for studying specific 5-HT circuits in a manner that anatomically and temporally approximates 5-HT transmission (Barnes and Sharp, 1999; Graeff et al., 1996; Steinbusch, 1981). Here, we integrate a range of approaches to clarify the contribution of the DRN→BA 5-HT pathway to fear.

Results

DRN→BA 5-HT pathway activity tracks fear

We visualised DRN 5-HT projections to the BA (DRN→BA 5-HT) and nucleus accumbens (NA) (DRN→NA 5-HT), two subcortical structures involved in fear-related and motivated behaviours. Transfection of fluorescent synaptophysin in DRN 5-HT neurons indicated projection terminals in the BA and NA, consistent with 5-HT immunofluorescence labelling (Steinbusch, 1981) (Figure 1A–C, S1A–B). To monitor pathway activity during behaviour, we used fibre photometry to image bulk calcium signal at 5-HT terminals by expressing GCaMP6(m) in a Cre-dependent manner in DRN 5-HT neurons of 5-HTT-Cre mice (Figure 1E–F). GCaMP6 expression was selective for 5-HT+ neurons (99.2±0.1 SEM % 5-HT+ of 503±60 SEM GCaMP6+ cells, n=2 mice) (Figure 1D, S1E–F). Optical fibres were implanted in the BA or NA to record projection activity (Figure 1G, S1C–D,G–H).

Mice underwent a 3-day task designed to produce robust but submaximal fear (Bukalo et al., 2015; Gunduz-Cinar et al., 2018), thereby permitting sufficient range to detect potentiating and attenuating effects. During fear conditioning (FC), mice learned to associate an auditory conditioned stimulus (CS) with a footshock (unconditioned stimulus, US), as evidenced by increased freezing across CS-US pairings (1-way RM ANOVA; BA $F(3,21)=5.45$, $p=0.006$; NA $F(3,24)=7.06$, $p=0.002$) (Figure 1H, S2C). Successful fear retrieval (FR) was evident in freezing during the first 5 of 50 CS presentations without US during fear extinction training (FE). Freezing decreased over CSs during FE (1-way RM-ANOVA; BA $F(10,70)=11.35$, $p<0.001$; NA $F(10,80)=4.84$, $p<0.001$) (Figure 1H, S2C). At extinction memory retrieval (ER), freezing recovered slightly but remained lower than at FR (ER, Wilcoxon test; BA, $W=36$, $p=0.008$; NA, $W=45$, $p=0.004$) (FE vs. ER, paired t-test; BA, $t(7)=3.66$, $p=0.008$; NA, $t(8)=2.31$, $p=0.049$) (Figure 1H, S2C).

Photometric recordings revealed correlates of 5-HT pathway activity during behaviour. Changes were considered significant if z-scored signal exceeded ±1.96 standard deviations (s.d.) of baseline. Over FC, there was a gradual, sustained fluorescence increase in DRN→BA 5-HT projections, but a non-significant decrease in DRN→NA projections

(Figure 1I, S2E). There were also transient rises in signal in the BA, but not NA, that were augmented with successive CS-US pairings (Figure S2A,F).

In the BA, area under the curve (AUC) of z-scored fluorescence for each CS was unaltered, relative to pre-CS baseline (BL), during the early and late halves (14.75 s) of CS1, but elevated during late CS2 and throughout CS3 (1-way RM ANOVA; CS1, $p>0.05$; CS2 $F(2,12)=52.72$, $p<0.001$, Sidak test [BL vs. early, $p>0.05$, BL vs. late, $p<0.001$; early vs. late, $p<0.001$]; CS3 $F(2,12)=56.99$, $p<0.001$, Sidak test [BL vs. early, $p<0.001$; BL vs. late, $p<0.001$; early vs. late, $p>0.05$) (Figure 1J). This progressively earlier increase is consistent with the accrual of associative strength to the CS, which in turn suggests a fear learning signal in the DRN→BA 5-HT pathway.

Fluorescence in the BA rose at FR, when freezing was also high, before decreasing along with freezing across FE (AUC of 180 s, 1-way RM ANOVA; $F(2,8)=7.21$, $p=0.016$, Sidak test [BL vs. CS1–5, $p>0.05$; BL vs. CS46–50, $p>0.05$, CS1–5 vs. CS46–50, $p=0.013$]) (Figure 1K–L). DRN→NA 5-HT activity showed no change over FR/FE (Figure S2G). Neither pathway displayed changes at ER (Figure S2B,H).

Analyses between DRN→BA 5-HT activity and freezing (Figure 1M) indicated fluorescence during the last FC CS correlated with freezing during subsequent FR (Pearson, $r^2=0.85$ $F(1,3)=17.04$, $p=0.026$) (Figure 1O). Additionally, higher fluorescence at FR predicted more freezing at ER the next day (Pearson, $r^2=0.84$, $F(1,3)=15.58$, $p=0.029$), and activity at ER correlated with concurrent freezing (Pearson, $r^2=0.60$, $F(1,6)=9.15$, $p=0.023$) (Figure 1P–Q). Fluorescence did not correlate with locomotor activity during pre-FC baseline (n=7 mice, Fisher mean $z=0.07$, reverse transformed $r=0.07$, $p>0.05$) (Figure 1N). Thus, DRN→BA 5-HT activity predicted fear memory expression and maintenance following FE. These same correlations were non-significant for DRN→NA 5-HT activity (Pearson; FC fluorescence vs. FE freezing, $r^2=0.00$, $p>0.05$; FE fluorescence vs. ER freezing, $r^2=0.10$, $p>0.05$; ER fluorescence vs. freezing, $r^2=0.23$, $p>0.05$) (Figure S2I–K).

To confirm DRN→BA 5-HT activity reflected fear and not a sensory artefact of repeated CSs, we conducted photometry during a discriminative FC task, in which mice learned to freeze to a CS predicting shock (CS+) but not to a neutral CS (CS-) (2-way RM ANOVA; CS# $F(5,15)=4.63$, $p=0.009$; CS type $p>0.05$; CS#×CS type $F(5,15)=4.98$, $p=0.007$; Sidak test, CS+ vs. CS-, FC [CS1 $p>0.05$, CS2 $p>0.05$, CS3 $p=0.002$], FR [CS1–5 $p=0.002$]) (Figure S1I). DRN→BA 5-HT activity increased during CS+ but not CS- (2-way RM ANOVA; CS# $F(5,15)=26.17$, $p<0.001$; CS type, $p>0.05$; CS#×CS type $F(5,15)=6.37$, $p=0.002$; Sidak test [CS+ vs. CS; FC, CS1 $p>0.05$, CS2 $p>0.05$, CS3 $p=0.002$; FR, CS1–5 $p=0.001$) (Figure S1J). Photometry performed in 5-HTT-Cre mice injected with Cre-dependent YFP rather than GCaMP6 (Figure S2D) indicated no change in DRN→BA or DRN→NA 5-HT fluorescence during testing (Figure S2L1–L3, M1–M3).

DRN→BA and DRN→NA 5-HT pathways are anatomically distinct

Differential recruitment of DRN→BA and DRN→NA 5-HT pathways during fear led us to ask whether these pathways are anatomically segregated. To determine the extent to which DRN neurons project to one or both regions, we injected the retrograde neuronal tracer,

cholera toxin B (CTb), conjugated to Alexa 488 or 555, into the BA and NA of wild-type mice (Figure 2A–C). There were similar numbers of BA- and NA-projecting cells labelled in the DRN (BA, 57±18 SEM cells, n=5 mice; NA, 51±26 SEM cells, n=5 mice) but almost no overlap, indicating distinct, non-collateralising populations (1-sample t-test, theoretical mean=0; BA only, $t(4)=3.87$, $p=0.018$; NA only, $t(4)=2.81$, $p=0.049$; both $p>0.05$) (Figure 2D–E). Co-injection of both CTb variants into the BA and NA indicated extensive fluorophore overlap in the DRN, confirming equivalent transfection efficacy (1-sample t-test, theoretical mean=0; 488 only $p>0.05$; 555 only $p>0.05$; both, $t(1)=34.66$, $p=0.018$) (Figure S3A–D).

Next, we tested whether anatomical segregation of DRN outputs to the BA and NA reflects affiliation with discrete neural information streams and distinct input sources. The cTRIO tracing method (Schwarz et al., 2015) was used to visualise neurons making synaptic connections onto DRN 5-HT neurons projecting to either the BA or NA. A retrogradely transfecting Cre-dependent FLPo construct was injected into the BA or NA, and a retrograde rabies virus, as well as accompanying FLPo-dependent starter viruses, injected into the DRN of 5-HTT-Cre mice (Figure 2F, S3E). Similar numbers of BA- and NA-projecting DRN 5-HT cells were transfected with starter virus (BA, 33±6 SEM TVA+ cells; NA, 50±18 SEM TVA+ cells; t-test $p>0.05$). GFP-labelled input cells were also equivalent between groups (DRN→BA, 561±315 SEM; DRN→NA, 958±484 SEM; t-test, $p>0.05$). In the absence of starter viruses, there was no rabies transfection (Figure S3F–G).

GFP-labelled inputs to BA- and NA-targeting 5-HT neurons were found within the DRN and various mid- and forebrain regions (Table S1). However, DRN→BA neurons received more input from the periaqueductal grey (PAG) (t-test, $t(600)=5.72$, $p<0.001$) and locus coeruleus (LC) (t-test, $t(600)=2.07$, $p=0.039$), whereas DRN→NA neurons were more heavily innervated by the ventral pallidum (VP) (t-test, $t(600)=2.92$, $p=0.004$) and local DRN inputs (t-test, $t(600)=5.94$, $p<0.001$) (Figure 2G–H). These differences are intriguing given the PAG and LC are implicated in fear and defensive behaviours, while the VP interacts with the NA to regulate reward-seeking (McCall et al., 2017; Richard et al., 2016; Tovote et al., 2015).

DRN→BA 5-HT pathway bidirectionally regulates fear

We next assessed the causal contribution of the DRN→BA 5-HT pathway to fear with *in vivo* optogenetics. DRN 5-HT neurons of 5-HTT-Cre mice were transfected with the excitatory opsin ChR2 and implanted with optical fibres in the BA (Figure 3A–C, S4A). ChR2 was selectively expressed in 5-HT+ neurons (DRN, 99.7±0.2 SEM % 5-HT+ of 334±56 SEM ChR2+ cells, n=3 mice) (Figure 3D). Blue light (20 Hz) was delivered at each FC CS (Figure 3G).

DRN→BA 5-HT excitation increased freezing during FC CS2 and CS3 (2-way RM ANOVA; time $F(3,54)=51.79$, $p<0.001$; opsin $F(1,18)=8.008$, $p=0.011$; time×opsin $F(3,54)=8.39$, $p<0.001$; Sidak test, ChR2 vs. YFP, BL $p>0.05$, CS1 $p>0.05$, CS2 $p<0.001$, CS3 $p=0.001$) (Figure 3H). Notably, light during CS1 (i.e. before any US) did not induce freezing or affect movement velocity (2-way RM ANOVA; time $F(3,42)=16.81$, $p<0.001$; opsin $p>0.05$; time×opsin $p>0.05$) (Figure S3H). Freezing was also higher in ChR2 mice

during light-free FR/FE (2-way RM ANOVA; time $F(2,36)=76.77$, $p<0.001$; opsin $F(1,18)=4.60$, $p=0.046$; time×opsin, $p>0.05$) and subsequent ER (2-way RM ANOVA; time $F(1,18)=110.50$, $p<0.001$; opsin $F(1,18)=16.15$, $p<0.001$; time×opsin $F(1,18)=18.19$, $p<0.001$; Sidak test, ChR2 vs. YFP, BL $p>0.05$, CS1–5 $p<0.001$) (Figure 3H). Fear potentiation was specific to the CS-US association because there was no group difference in freezing during re-exposure to the conditioning context (t-test $p>0.05$). When DRN→BA 5-HT excitation was paired with CSs without USs, freezing was absent (FR, 2-way RM ANOVA; FR time $p>0.05$, opsin $p>0.05$, time×opsin $p>0.05$) (Figure S3J).

We next assessed effects of DRN→BA 5-HT inhibition during FC by transfecting DRN 5-HT neurons with the inhibitory opsin iC++ and implanting optical fibres to shine continuous blue light in the BA during FC CSs (Figure 3A,E–G, S4B). YFP controls in the excitation and inhibition experiments showed similar freezing at all stages (2-way RM ANOVA; FC [time $F(3,54)=22.46$, $p<0.001$; group $p>0.05$; time×group $p>0.05$], FE [time $F(2,36)=239.00$, $p<0.001$; group $p>0.05$; time×group $p>0.05$], ER [time $F(1,18)=80.30$, $p<0.001$; group $p>0.05$, time×group $p>0.05$]) (t-test, context retrieval $p>0.05$).

Inhibition did not alter freezing at FC (2-way RM ANOVA; time $F(3,45)=20.93$, $p<0.001$; opsin $p>0.05$; time×opsin $p>0.05$) or movement velocity during the first FC CS (2-way RM ANOVA; time $F(3,39)=29.51$, $p<0.001$; opsin $p>0.05$; time×opsin $p>0.05$) (Figure S3I). However, iC++ mice had lower freezing at light-free FR (2-way RM ANOVA; time $F(2,30)=74.89$, $p<0.001$; opsin $F(1,15)=7.01$, $p=0.018$; time×opsin $F(2,30)=6.11$, $p=0.006$; Sidak test, ChR2 vs. YFP, BL $p>0.05$, CS1–5 $p<0.001$, CS46–50 $p>0.05$) (Figure 3I) and ER (2-way RM ANOVA; time $F(1,15)=57.19$, $p<0.001$; opsin $F(1,15)=4.66$, $p=0.048$; time×opsin $F(1,15)=5.48$, $p=0.034$; Sidak test, ChR2 vs. YFP, BL $p>0.05$, CS1–5 $p=0.007$). Attenuation was selective for CS fear memory formation, since context fear was normal (t-test $p>0.05$) (Figure 3I). Combined, our optogenetic excitation and inhibition data demonstrate a causal, bidirectional role for the DRN→BA 5-HT pathway in fear.

DRN→BA 5-HT pathway bidirectionally regulates fear extinction

Fear and extinction involve shared but partly dissociable neural circuits (Milad and Quirk, 2012). DRN→BA 5-HT manipulations during FC altered the strength of fear memory, producing effects that persist after FE, but this does not directly address the pathway's role in extinction memory formation. Mice therefore underwent FC (ANOVA; ChR2 time $F(3,45)=73.40$, $p<0.001$; opsin $p>0.05$ time×opsin $p>0.05$; iC++ time $F(3,57)=30.38$, $p<0.001$; opsin $p>0.05$, time×opsin $p>0.05$) and optogenetic excitation or inhibition of DRN→BA 5-HT projections during each FE CS, followed by ER, light-free, the next day (Figure 3J,L, S5A–B). YFP controls in both experiments froze similarly at FC (2-way RM ANOVA; time $F(3,48)=46.62$, $p<0.001$; group $p>0.05$; time×group $F(3,48)=1.24$, $p>0.05$) and ER (2-way RM ANOVA; time $F(1,16)=121.10$, $p<0.001$; group $p>0.05$; time×group $p>0.05$), but YFP controls for iC++ mice froze more than for ChR2 at FE (2-way RM ANOVA; time $F(10,160)=6.45$, $p<0.001$; group $F(1,16)=5.52$, $p=0.032$; time×group, $p>0.05$).

Optogenetic excitation did not alter fear during FE (2-way RM ANOVA; time $F(10,150)=10.21$, $p<0.001$; opsin $p>0.05$; time×opsin $p>0.05$) (Figure 3K) but increased

freezing at ER (2-way RM ANOVA; time $F(1,15)=71.64$, $p<0.001$; opsin $F(1,15)=10.71$, $p=0.005$; time×opsin $F(1,15)=10.7$, $p=0.005$; Sidak test, ChR2 vs. YFP, BL $p>0.05$, CS1–5 $p<0.001$) (Figure 3K). Conversely, optogenetic inhibition during FE decreased freezing at ER (2-way RM ANOVA; time $F(1,19)=197.90$, $p<0.001$; opsin $F(1,19)=15.92$, $p=0.001$; time×opsin $F(1,19)=25.41$, $p<0.001$; Sidak test, iC++ vs. YFP, BL $p>0.05$, CS1–5 $p<0.001$) without affecting FE (2-way RM ANOVA; time $F(10,190)=4.38$, $p<0.001$; opsin $p>0.05$; time×opsin $p>0.05$) (Figure 3L). These observations show DRN→BA 5-HT projections bidirectionally affect extinction memory formation and, taken together with the effects of FC manipulations, suggest recruitment of this pathway biases in favour of fear during initial fear learning and subsequent extinction.

DRN→BA 5-HT pathway sculpts BA fear-encoding

We next combined *in vivo* optogenetics and electrophysiological recordings to test if the DRN→BA 5-HT pathway regulates fear by modifying BA neuronal fear-encoding. DRN 5-HT neurons were transfected with ChR2 and optical fibres and electrode arrays implanted in the BA to excite 5-HT inputs during FC CSs while simultaneously recording BA neuronal activity (Figure 4A–D, S6A).

Freezing was not elevated in the ChR2 group during FC (2-way RM ANOVA; time $F(3,48)=25.96$, $p<0.001$; opsin $p>0.05$, time×opsin $p>0.05$) (Figure S3K), but was higher at light-free FR (2-way RM ANOVA; time $F(2,32)=30.67$, $p<0.001$; opsin $p>0.05$; time×opsin $F(2,32)=6.09$, $p=0.006$; Sidak test, ChR2 vs. YFP, BL $p>0.05$, CS1–5 $p<0.001$, CS46–50 $p>0.05$) and ER (2-way RM ANOVA; time $F(1,16)=58.49$, $p<0.001$; opsin $F(1,16)=10.92$, $p=0.005$; time×opsin $F(1,16)=14.23$, $p=0.002$; Sidak test, ChR2 vs. YFP, BL $p>0.05$, CS1–5 $p<0.001$) (Figure S3K).

We classified neurons as CS-responsive if z-scored mean firing during CS-pips exceeded ±2.58 s.d. of pre-CS-pip baseline in two consecutive 0.01 s time bins (Halladay and Blair, 2015) (Figure 4E). The proportion of CS-responsive cells did not differ between ChR2 and YFP mice at FC (Fisher's $p>0.05$) (Figure 4F1). Though neither group deviated from baseline, mean z-scored firing of all recorded units was lower in ChR2 mice (2-way RM ANOVA; time $F(24,2616)=3.10$, $p<0.001$; opsin $p>0.05$; time×opsin $F(24,2616)=2.04$, $p=0.002$; Sidak test, ChR2 vs. YFP, 0.02 s $p=0.020$) (Figure 4F2). This excitation-driven reduction in firing accords with *ex vivo* data showing inhibition of BA output neurons by 5-HT (Bocchio et al., 2015; Jiang et al., 2009; Rainnie, 1999; Sengupta et al., 2017).

At light-free FR, CS-evoked firing was elevated from baseline in both groups (2-way RM ANOVA; time $F(24,3912)=15.19$, $p<0.001$; opsin $p>0.05$; time×opsin, $p>0.05$) (Figure 4G2). However, the proportion of CS-responsive neurons was greater in the ChR2 group, which also froze more than YFP controls (chi-square test, $\chi^2(2)=6.691$, $p=0.035$) (Figure 4G1). Furthermore, activity across the 5 FR CSs differed between groups (chi-square test, $\chi^2(3)=7.993$, $p=0.046$) (Figure 5A1–A5); ChR2 mice had a greater proportion of neurons exhibiting sustained excitation across CS1–5 (ChR2 31%, YFP 17%), while a greater proportion in YFP controls increased across CSs (ChR2 3%, YFP 11%).

The proportion of CS-responsive neurons was similar between groups at ER (chi-square test $p>0.05$) (Figure 4I1), but mean CS-related firing was increased from baseline in ChR2, not YFP, mice, again mirroring higher freezing (2-way RM ANOVA; time $F(24,3792)=10.69$, $p<0.001$; opsin $p>0.05$; time×opsin $F(24,3792)=2.51$, $p<0.001$; Sidak test, ChR2 vs. YFP, 0.12 s $p=0.048$, 0.13 s $p<0.001$) (Figure 4I2).

We then examined whether DRN→BA 5-HT excitation altered BA neuronal responses at the start of a freezing episode. The proportion of freezing onset-responsive neurons (z-scored mean firing rate during the first 1 s of a freezing episode that exceeded ±1.96 s.d. of pre-freezing baseline in a 0.1 s time bin) did not differ between groups during any test phase (FC, chi-square test $p>0.05$; FE, Fisher's $p>0.05$; ER, chi-square test $p>0.05$) (Figure 4H1, S6B1,C1). However, mean z-scored firing of all recorded neurons was higher in ChR2 mice during freezing onset at FR (2-way RM ANOVA; time $F(10,1300)=3.01$, $p<0.001$; opsin $F(1,130)=4.206$, $p=0.042$; time×opsin $F(10,1300)=5.14$, $p<0.001$) and ER (2-way RM ANOVA; time $F(10,1240)=3.08$, $p<0.001$; opsin $p>0.05$; time×opsin $F(10,1240)=4.93$, $p<0.001$; Sidak test, ChR2 vs. YFP, 0.3 s $p<0.001$), but not FC (2-way RM ANOVA; time, $p>0.05$; opsin $p>0.05$; time×opsin $p>0.05$) (Figure 4H2, S6B2,C2).

Together these findings demonstrate the fear-potentiating effects of exciting DRN→BA 5-HT projections are associated with a strengthening of BA neuronal encoding of fear.

DRN→BA 5-HT pathway accentuates fear-related BA theta power

Fear states are reflected in patterns of synchronous BA neuronal firing, particularly oscillations in the theta range (Bocchio et al., 2017; Karalis et al., 2016; Likhtik et al., 2014; Seidenbecher, 2003). Examining BA local field potentials (LFPs) in the context of DRN→BA 5-HT excitation during FC (Figure 5B) revealed differences in power spectral densities between ChR2 and YFP mice during CSs at all test phases (2-way RM ANOVA; FC CS3 [frequency $F(31,496)=62.19$, $p<0.001$; opsin $F(1,16)=3.88$, $p=0.067$; frequency×opsin $F(31,496)=5.12$, $p<0.001$], FR CS1–5 [frequency $F(31,465)=50.34$, $p<0.001$; opsin $p>0.05$; frequency×opsin $F(31,465)=5.61$, $p<0.001$], ER CS1–5 [frequency $F(31,496)=62.52$, $p<0.001$; opsin $p>0.05$; frequency×opsin $F(31,496)=2.15$, $p<0.001$]) (Figure 5C–E). Differences were absent at pre-CS FE baseline, confirming spectral density differences were CS-related (2-way RM ANOVA; frequency $F(31,465)=45.96$, $p<0.001$; opsin $p>0.05$; frequency×opsin $p>0.05$) (Figure S7G).

Specifically, excitation increased theta power by FC CS3 (t-test; CS1 $p>0.05$; CS2 $p>0.05$; CS3, $t(16)=3.63$, $p=0.002$) (Figure 6A–C) and during light-free FR and ER, when freezing was elevated (t-test; FE CS1–5, $t(15)=4.55$, $p<0.001$; ER CS1–5, $t(16)=2.24$, $p=0.040$) (Figure 6D, S7H). Delta power was less in ChR2 mice during FC CS3 (t-test; CS1 $p>0.05$; CS2 $p>0.05$; CS3, $t(16)=3.26$, $p=0.005$) (Figure 6A–C) and FR (Mann Whitney test, $U=14$, $p=0.036$) (Figure 6D), but not ER (t-test $p>0.05$) (Figure S7H). By contrast, alpha and beta oscillations were similar at FC (t-test; alpha, CS1 $p>0.05$, CS2 $p>0.05$, CS3 $p>0.05$; beta CS1 $p>0.05$, CS2 $p>0.05$, CS3 $p>0.05$), FR (t-test; alpha $p>0.05$, beta $p>0.05$), and ER (t-test; alpha $p>0.05$, beta $p>0.05$) (Figure 6A–D, S7H). Freezing during FR correlated with both theta power and mean unit firing in ChR2 mice (Pearson; theta, $r^2=0.74$ $F(1,5)=14.58$,

p=0.012; firing rate, r^2=0.66 F(1,5)=9.85, p=0.026), but only with firing in YFP mice (Pearson; theta, r^2=0.14, p>0.05; firing rate, r^2=0.54 F(1,6)=7.14, p=0.037) (Figure 6E–F).

We therefore examined the timing of neuronal firing with respect to theta power (Figure 6GH). For both groups, the proportion of BA neurons phase-locked to theta was greater during the first FR CS than the last FC CS (Fisher's, ChR2 p<0.001, YFP p<0.001) (Figure 6I). However, the proportion of theta-locked cells was higher in ChR2 than YFP mice at FC (Fisher's p=0.049) and FR (Fisher's p=0.024). When trials were shuffled between FC and FR so that CS-related unit spiking in one test phase was compared against CS-related theta oscillations in the other, phase-locking effects were absent (Fisher's for all comparisons p>0.05). This indicates increased phase-locking is not an artefact of higher firing frequency or theta power but a change in the temporal code of neuronal firing.

Fear-activated DRN→BA 5-HT neurons co-express a glutamate marker

Given the presence of co-transmitters in DRN 5-HT neurons (Fu et al., 2010), we assessed the neurochemical identity of BA-projecting DRN neurons by injecting CTb into the BA of wild-type mice. Labelled BA-projecting neurons were concentrated medially in the middle to caudal DRN, an area also highly immunoreactive for 5-HT and the glutamatergic marker VGluT3 (Figure 7A–F). We subjected CTb-injected mice to FC (or context exposure) and immunostained for the neuronal activity marker c-Fos, along with 5-HT and VGluT3 (Figure 7H). There were equal numbers of CTb+ cells in the two groups (FC, 50.0±3.2 SEM cells, n=6 mice; context, 50.3±2.3 SEM cells, n=6 mice). Of the BA-projecting DRN neurons, the majority contained both 5-HT and VGluT3 (2-way RM ANOVA; marker F(2,20)=675.30, p<0.001; group p>0.05; marker×group p>0.05; Sidak test, 5-HT vs. VGluT3 p>0.05, 5-HT vs. 5-HT/VGluT3 p<0.001, VGluT3 vs. 5-HT/VGluT3 p<0.001) (Figure 7I). There was a greater proportion of c-Fos+ projection cells co-expressing 5-HT and VGluT3 in FC mice (2-way RM ANOVA; marker F(2,20)=35.04. p<0.001; group F(1,10)=14.27, p=0.004; marker×group F(2,20)=13.45, p<0.001; Sidak test, FC vs. context, 5-HT/c-Fos p>0.05, VGluT3/c-Fos p>0.05, 5-HT/VGluT3/c-Fos p<0.001) (Figure 7I).

DRN neurons are also GABAergic and catecholaminergic (Fu et al., 2010). Using transgenic mice to express GFP under the control of the GABA-synthesizing enzyme (GAD2) or dopamine transporter (DAT) gene, we saw almost no GAD2 or DAT expression in CTb-labelled BA-projecting DRN cells (Figure 7G, S7A–C). CTb-labelled cell numbers were equivalent across groups (GAD2, 66.5±7.3 SEM cells, n=6 mice; DAT, 65.4±5.4 SEM cells, n=5 mice). GAD2+ cells were most dense in the lateral DRN, whereas DAT+ cells were in the rostral DRN and ventral tegmental area (VTA) (Figure S7A–D). Immunostaining for the noradrenaline-catalysing enzyme dopamine β-hydroxylase (DBH) in wild-type mice revealed locus coeruleus but not DRN cell-labelling, as reported previously (Nagatsu et al., 1979) (Figure S7E–F).

Thus, the DRN→BA pathway is comprised of neurons co-expressing 5-HT and a glutamatergic marker, which suggests its fear-modulating role could occur through glutamate and/or 5-HT transmission in the BA. Indeed, VGluT3 immunoreactivity was evident in BA 5-HT+ axons transfected with ChR2 in 5-HTT-Cre mice (Figure 7J).

DRN→BA pathway regulates fear via BA 5-HT-Rs

To test if 5-HT signalling is necessary for the fear-modulating influence of the DRN→BA 5-HT pathway, we infused a cocktail of 5-HT_{1A} and 5-HT_{2A} receptor antagonists, or vehicle (VEH), into the BA prior to ChR2-driven pathway-excitation at FC (Figure 7K–M, S7I). We chose these 5-HT-R subtypes because they functionally modulate BA neurons and regulate fear-related behaviour (Bocchio et al., 2015; Jiang et al., 2009; Li et al., 2006; Matsuzaki et al., 2011; Rainnie, 1999; Sengupta et al., 2017).

Overall, ChR2 mice froze more than YFP counterparts by FC CS3 (3-way RM ANOVA; time $F(3,78)=61.72$, $p<0.001$; main effect of opsin $F(1,26)=3.57$, $p=0.070$; time×opsin $F(3,78)=4.72$, $p=0.004$; Sidak test, ChR2 vs. YFP, CS3 $p=0.015$) (Figure 7N). 5-HT-R antagonism reduced FC freezing across both opsin groups (drug $F(1,26)=54.07$, $p<0.001$; time×drug $F(3,78)=15.62$, $p<0.001$; Sidak test, drug vs. VEH, CS2 $p=0.001$, CS3 $p<0.001$; time×opsin×drug, $p>0.05$).

At light/drug-free FR/FE, only VEH-treated ChR2 mice froze more than YFP mice during FR, and drug reduced freezing in both opsin groups (3-way RM ANOVA; time $F(2,52)=42.67$, $p<0.001$; opsin $F(1,26)=4.55$, $p=0.043$; drug $F(1,26)=26.33$, $p<0.001$; time×opsin $F(2,52)=5.78$, $p=0.005$; time×drug $F(2,52)=26.45$, $p<0.001$; time×opsin×drug $F(2,52)=3.64$, $p=0.033$; Sidak test, ChR2 vs. YFP, CS1–5 VEH $p=0.006$, CS1–5 drug $p>0.05$; drug vs. VEH, CS1–5 YFP $p=0.033$, CS1–5 ChR2 $p<0.001$) (Figure 7N). The same pattern of ChR2-driven fear potentiation, and its absence after 5-HT-R antagonism, was evident at ER (3-way RM ANOVA; time $F(1,26)=125.43$, $p<0.001$; opsin $F(1,26)=18.39$, $p<0.001$; drug $F(1,26)=88.45$, $p<0.001$; time×opsin $F(1,26)=17.77$, $p<0.001$; time×drug $F(1,26)=84.20$, $p<0.001$; time×opsin×drug $F(1,26)=6.76$, $p=0.015$; Sidak test, ChR2 vs. YFP, CS1–5 VEH $p<0.001$, CS1–5 drug $p>0.05$; drug vs. VEH CS1–5 YFP $p<0.001$, CS1–5 ChR2 $p<0.001$) (Figure 7N).

These data show 5-HT transmission is an obligatory substrate for the DRN→BA 5-HT pathway's fear-potentiating effects, though they do not exclude a potential contribution of co-released glutamate cannot be excluded.

DRN→BA pathway is positioned to orchestrate a broader fear network

Fear memory is mediated by a wide network of interacting brain regions (Bocchio et al., 2017; Herry and Johansen, 2014). To delineate projection patterns of DRN→BA 5-HT neurons and the degree to which they collateralise to regions other than the BA, we injected a retrogradely-transfecting Cre-recombinase virus into the BA and a Cre-dependent virus containing terminal-labelling fluorescent synaptophysin into the DRN of wild-type mice (Figure 8A, S8B). Labelled somata were restricted to the DRN (Figure S8C1–C2). To compare against overall DRN 5-HT terminal labelling, Cre-dependent synaptophysin was injected into the DRN of 5-HTT-Cre mice (Figure 8A, S8A).

Total fluorescence across the brain was higher in the DRN-wide- (89.2±10.3 SEM) relative to the DRN→BA pathway-labelled group (27.2±6.0 SEM) (t-test, $t(4)=5.22$, $p=0.006$). Relative labelling in the BA was higher with pathway-restricted transfection (t-test, $t(56)=30.36$, $p<0.001$) (Figure 8B–C). Collaterals from BA-projecting DRN neurons were

visible but sparse in regions including the NA ($t(56)=3.70$, $p<0.001$), dorsal striatum ($t(56)=2.25$, $p=0.028$), VTA ($t(56)=9.45$, $p<0.001$), LC ($t(56)=2.99$, $p=0.004$), and lateral hypothalamus ($t(56)=6.78$, $p<0.001$) (Figure 8B–C), suggesting these projections are largely faithful to the DRN→BA pathway.

We then mapped anatomical targets of BA neurons receiving DRN input by injecting wild-type mice with an anterograde, trans-synaptic Cre-recombinase virus into the DRN and Cre-dependent YFP into the BA (Zingg et al., 2017) (Figure 8D–E). YFP+ fibres originating from DRN-innervated BA neurons were visible in target regions implicated in fear, including the medial prefrontal cortex (mPFC), bed nucleus of the stria terminalis (BNST), PAG, ventral hippocampus, and central amygdala (CeA) (Herry and Johansen, 2014; Rajmohan and Mohandas, 2007) (Figure 8F–G). Hence, BA neurons receiving DRN input have diffuse targets throughout the known fear network.

Discussion

We aimed to characterise how the 5-HT system modulates the BA to regulate learned fear behaviour. We found fear selectively recruits DRN→BA 5-HT projections and described the pathway's bidirectional involvement in potentiating fear and impairing extinction memory. We established the capacity of the DRN→BA 5-HT pathway to calibrate fear-associated neuronal firing and theta power in the BA. Despite co-expressing a glutamate marker, DRN projections to the BA regulate fear via 5-HT signalling at 5-HT_{1A} and 5-HT_{2A} receptors. Finally, we positioned the DRN→BA 5-HT pathway within a wider network of brain circuits that subserves fear.

DRN→BA 5-HT pathway facilitates fear memory

Previous studies have shown DRN 5-HT neurons are quiescent during sleep and active during emotionally salient events, such as aversive stimuli (Allers and Sharp, 2003; Baratta et al., 2016; Cohen et al., 2015; Grahn et al., 1999; Hajós et al., 2007; Kocsis et al., 2006; Li et al., 2016; Sakai, 2011; Schweimer and Ungless, 2010; Seo et al., 2019; Spannuth et al., 2011; Takase et al., 2004). We showed the specific DRN→BA 5-HT pathway is sufficient for driving acute 5-HT-mediated fear regulation (Burghardt et al., 2004; Marcinkiewcz et al., 2016). In contrast, chronic enhancement of 5-HT signalling may attenuate fear by causing receptor desensitisation and downregulation over time (Bosker et al., 2001; Burghardt et al., 2004; Machado-Vieira et al., 2010), and developmental 5-HT function may shape fear behaviour through entirely separate, temporally restricted mechanisms (Ansorge et al., 2004; Rebello et al., 2014). Pharmacology and chemical lesion data corroborate disrupting 5-HT in the BA impacts fear (Baratta et al., 2016; Christianson et al., 2010; Izumi et al., 2012; Johnson et al., 2015; Li et al., 2006; Liang, 1999; Matsuzaki et al., 2011).

Engagement of the DRN→BA 5-HT pathway not only strengthened fear during FC but also impaired FE memory formation. Thus, the pathway promotes fear rather than facilitating the type of learning predominant at a given test phase. Given fear and extinction memories are associated with separate neuronal populations in the BA, DRN 5-HT inputs might bias BA neuronal activity in favour of fear-encoding. In support of this, DRN→BA 5-HT excitation produced sustained BA neuronal excitability, in accordance with putative 'fear neurons'

(Herry et al., 2008; Senn et al., 2014). The mechanism by which DRN 5-HT inputs facilitate fear ensembles remains a key question for future studies, but could relate to differential 5-HTR subtype expression or the gating of other BA inputs via axo-axonic 5-HT synapses (Cheng et al., 1998; Guo et al., 2017; Muller et al., 2007; Yamamoto et al., 2012).

Functional mechanisms of 5-HT modulation in the BA during fear

Fear states have been linked to elevated neuronal firing and theta power in the BA (Barkus et al., 2014; Johansen et al., 2010; Karalis et al., 2016; Likhtik et al., 2014; McHugh et al., 2014). For example, genetically induced 5-HTT deficiency, which leads to increased fear and higher extracellular 5-HT, enhances theta power; in contrast, 5-HTT overexpression associates with less fear, lower 5-HT levels, and reduced theta (Barkus et al., 2014; Narayanan et al., 2011). We demonstrated DRN→BA 5-HT excitation increased fear-associated neuronal firing on days following optogenetic excitation, suggesting 5-HT affects rate coding. In addition, enhanced phase-locking to theta during CS presentations was consistent with an effect of 5-HT inputs on temporal coding in the BA, suggesting 5-HT regulates the timing of neuronal firing with respect to local network activity. Thus, the decrease in BA neuronal firing produced by 5-HT input excitation during FC may have evolved, via the facilitation of plasticity arising from enhanced theta oscillations, into elevated firing rates in subsequent test sessions (Bazelot et al., 2015; Chen et al., 2003).

Theta oscillations are amenable to modulation by 5-HT in several ways. BA principal neurons resonate at theta frequencies due to intrinsic membrane conductances, which could be affected by 5-HT-R signalling cascades (Pape and Driesang, 1998). Furthermore, parvalbumin interneurons are modulated by 5-HT and regulate BA oscillations (Bocchio et al., 2015; Davis et al., 2017). 5-HT transmission may also shape BA neuronal fear-encoding by gating other inputs to the BA, which accords with 5-HT input to the BA being insufficient to generate a fear memory in the absence of the US and with prior *ex vivo* accounts (Cheng et al., 1998; Guo et al., 2017; Yamamoto et al., 2012). 5-HT afferents are ideally positioned to modulate other inputs to the BA because more than half of 5-HT terminal boutons form heterosynaptic triads with the pre- and post-synaptic sites of other synapses (Belmer et al., 2017). By regulating theta oscillations, 5-HT transmission could gate the strength of other extrinsic inputs via heterosynaptic plasticity in the BA (Bazelot et al., 2015). The critical inputs are yet undefined, but a likely candidate is the mPFC, which entrains BA theta rhythms during fear (Karalis et al., 2016; Likhtik et al., 2014).

DRN→BA 5-HT pathway is functionally and anatomically distinct

DRN 5-HT neuron activity has been linked to a range of behavioural processes in addition to fear, including reward, sleep/wake states, movement, spatial memory, and cognitive flexibility (Cohen et al., 2015; Correia et al., 2017; Matias et al., 2017; Sakai and Crochet, 2001; Teissier et al., 2015; Teixeira et al., 2018). One mechanism by which 5-HT signalling might achieve such functional diversity with relatively high fidelity is through anatomical segregation of 5-HT output pathways (Graeff et al., 1996). In support of this notion, 5-HT inputs to the BA, BNST, and CeA are implicated in fear, whereas DRN projections to the NA and orbitofrontal cortex (OFC) mediate reward-related behaviours; 5-HT pathways projecting to distinct targets also receive inputs from different upstream regions (Li et al.,

2016; Marcinkiewcz et al., 2016; Ren et al., 2018). In particular, DRN→BA 5-HT projections receive inputs from other fear- and stress-associated regions, such as the PAG and LC, while reward-related areas, such as the VP, target NA-projecting DRN 5-HT neurons (Johansen et al., 2010; Ogawa et al., 2014; Pollak Dorocic et al., 2014; Richard et al., 2016; Weissbourd et al., 2014). Though 5-HT axons often collateralise to multiple targets, we found BA-projecting DRN neurons did not densely innervate other structures, consistent with earlier data (Fernandez et al., 2016; Gagnon and Parent, 2014). This unique pattern of inputs and outputs positions the DRN→BA 5-HT circuit within a broader fear network. These data, together with recent findings (Ren et al., 2018), suggest functional segregation across anatomically defined 5-HT pathways may be a common motif of the 5-HT system.

Additionally, DRN 5-HT neurons display heterogeneity at the level of gene expression and neurochemical phenotype (Bang et al., 2012; Hale and Lowry, 2011; Vasudeva et al., 2011). The molecular identity of individual neurons follows a topography within the DRN, as does the organisation of DRN projections according to anatomical targets (Fernandez et al., 2016; Vasudeva et al., 2011). These patterns may be established during development (Calizo et al., 2011; Deneris and Gaspar, 2018), such that 5-HT neurons could be assigned to functional pathways through a combination of genetic and migratory factors early in life. For instance, DRN projections to the CeA are devoid of VGluT3 (Ren et al., 2018), whereas we found the majority of BA-projecting DRN neurons are not only 5-HTergic, congruent with prior data (Ma et al., 1991), but most also contain VGluT3. This illustrates the remarkable degree to which DRN outputs are delineated according to molecular and anatomical identity.

Neurotransmission of DRN→BA 5-HT pathway during fear

Though most somata of 5-HT inputs to the BA contained VGluT3, VGluT3 co-localisation is more prominent in 5-HT somata than axonal fibres and may primarily assist in vesicular packaging of 5-HT (Amilhon et al., 2010; Gagnon and Parent, 2014). However, glutamate co-release from 5-HT neurons has been demonstrated, albeit *in vitro* (Johnson, 1994; Liu et al., 2014; Ren et al., 2018; Sengupta et al., 2017; Varga et al., 2009; Wang et al., 2019), raising the prospect of DRN→BA 5-HT neurons regulating fear via co-released glutamate. We provided evidence against this by blocking 5-HT-Rs in the BA to occlude fear-potentiating effects of DRN→BA 5-HT pathway excitation. Moreover, similar high-frequency optogenetic activation of BA 5-HT inputs *ex vivo* favours 5-HT over glutamate transmission (Sengupta et al., 2017). Since DRN 5-HT neurons are more active during emotionally salient events, these data imply 5-HT signalling may be the dominant mode of transmission in the DRN→BA 5-HT pathway during fear (Allers and Sharp, 2003; Cohen et al., 2015; Hajós et al., 2007; Kocsis et al., 2006; Li et al., 2016; Sakai, 2011; Schweimer and Ungless, 2010). Further investigation is warranted to clarify the presence and necessity of *in vivo* glutamate co-release in this circuit.

Conclusions

The 5-HT system is a major target for treatments for disorders characterised by pathological fear and is perturbed by a range of environmental, pharmacological, and genetic factors (Baratta et al., 2016; Lopreato et al., 2003; Smith et al., 2004). By identifying a key 5-HT

circuit that functions to calibrate the strength of fear memory and its resistance to extinction, the current study could provide novel insight into how pathological fear is instantiated and sustained. This could help to clarify individual differences in risk for affective illness and to serve to refine the development of new 5-HT-based therapeutics (Vasa et al., 2006).

STAR Methods

CONTACT FOR REAGENT AND RESOURCE SHARING

Further information and requests for resources and reagents should be directed to and will be fulfilled by the Lead Contact, Andrew Holmes (holmesan@mail.nih.gov).

EXPERIMENTAL MODEL AND SUBJECT DETAILS

5-HTT-Cre+/− (5-HTT-Cre) mice (MMRRC, B6.Cg-Tg(Slc6a4-cre)Et33Gsat, stock no. 031028-UCD) were maintained by crossing heterozygote males with wild-type C57BL/6J females (JAX 000664). Glutamate decarboxylase (GAD2)-GFP mice were generated by crossing Cre-dependent ROSA(EGFP-L10a) males (B6;129S4-Gt(ROSA)26Sor<tm9(EGFP/Rpl10a)Amc>/J; JAX 024750) with GAD2-IRES-Cre+/−females (STOCK Gad2<tm2(cre)Zjh>/J; JAX 010802) to generate a transgenic reporter line in which GABAergic cells were labelled with GFP. DAT-GFP mice were generated by crossing Cre-dependent ROSA(EGFP-L10a) males with DAT-Cre+/− females (B6.SJLSlc6a3<tm1.1(cre)Bkmn>/J; JAX 006660) to generate a transgenic reporter line in which dopaminergic cells were labelled with GFP. 5-HTT-Cre, GAD2-GFP, and DAT-GFP mice were genotyped by Transnetyx (Cordova, TN). Experiments not requiring Cre recombination used the 5-HTT-Cre−/− littermates (wild-types) of 5-HTT-Cre mice. Males and females were used. Assignment to experimental conditions was counterbalanced based on sex, age, and parents. Mice were singly-housed after surgeries to facilitate recovery and maintain the integrity of intracranial implants, with *ad libitum* access to food and water in a 12/12 h light/dark cycle (lights on 6am). Mice were at least 2 months old at the time of surgery, and between 3 and 6 months at the time of behavioural procedures. Experiments were performed in compliance with the National Institutes of Health Guide for the Care and Use of Laboratory Animals and approved by the local National Institute on Alcohol Abuse and Alcoholism Animal Care and Use Committee.

METHOD DETAILS

Surgical procedures

Stereotaxic surgery and targeting coordinates: Anaesthesia was induced at 3% isoflurane in oxygen (2 L/min) and maintained at 1–2%. Mice were placed in a stereotactic frame (Kopf Instruments) for injections and implantations. The DRN was targeted at anteroposterior (AP) −4.50 mm, mediolateral (ML) ±0.0 mm from bregma, and dorsoventral (DV) −2.20 mm from brain surface. The BA was targeted at AP −1.80 mm, ML ±3.15 mm, DV −4.90 mm from bregma for fibre implants, at DV −4.10 for cannulation, and at DV −5.15 for injections. The NA (specifically, the shell region) was targeted at AP +1.70, ML ±1.38, DV −4.70 from bregma for fibre implants, and at DV −4.90 for injections, at an angle of 10°. Intracerebral injections were delivered at 100 nL/min using glass pipettes, which

then remained at the injection site for 8 min to allow for diffusion before retracting. Mice were administered 5 mg/kg ketoprofen for post-operative analgesia.

In vivo fibre photometry: An adeno-associated viral (AAV) vector containing the Cre recombinase-dependent fluorescent calcium indicator, GCaMP6 (AAVdj-EF1a-DIO-GCaMP6m) (0.6 μL, Stanford University Neuroscience Gene Vector and Virus Core), or control reporter YFP (AAV2-EF1a-DIO-EYFP) (0.6 μL, UNC Vector Core) was injected into the DRN of 5-HTT-Cre mice. Optical fibres attached to metal ferrules (400 μm, 0.48 numerical aperture, Doric Lenses) were implanted unilaterally into the BA or NA and affixed with dental cement (Coralite Dental Products) to deliver and collect light. The implantation hemisphere was counterbalanced (BA, left n=4 mice, right n=4 mice; NA, left n=4 mice, right n=5 mice). Experiments were conducted 8 weeks after surgery.

In vivo optogenetics: AAV vectors containing Cre recombinase-dependent light-gated opsins were injected into the DRN of 5-HTT-Cre mice. The excitatory opsin, channelrhodopsin 2 (ChR2) (AAV2-EF1a-DIO-hChR2(E123T/T159C)-EYFP) (0.6 μL, University of North Carolina Vector Core), or the inhibitory opsin, iC++ (AAV2-EF1a-DIO-iC++-EYFP) (0.6 μL, University of North Carolina Vector Core), was used. For control groups, Cre recombinase-dependent YFP (AAV2-EF1a-DIO-EYFP) (0.6 μL, UNC Vector Core) was used. Optical fibres attached to ceramic ferrules (200 μm, 0.39 numerical aperture, Thorlabs) were implanted bilaterally into the BA and affixed with dental cement to deliver light stimulation. Experiments were conducted 5 weeks after surgery.

Combined in vivo optogenetics and neuronal recordings: An AAV viral vector containing Cre-dependent ChR2 or YFP was injected into the DRN of 5-HTT-Cre mice. Optrode arrays were constructed by affixing optical fibres attached to ceramic ferrules (200 μm, 0.39 numerical aperture) onto an 8×2–row array (200-μm spacing between rows) of tungsten microelectrodes (Innovative Neurophysiology), such that the fibre tip was aligned ~0.5 mm above the electrode tips. The optrode array assembly was positioned lengthwise anteroposterior (35-μm diameter electrode tips, 150-μm spacing between electrodes within a row). The optrode array was inserted into the BA unilaterally (coordinates for the most posterior and lateral electrode of the array; AP −2.20 mm, ML ±3.10 mm, DV −5.10), with counterbalancing for hemispheres (YFP, left n=4 mice, right n=5 mice; ChR2, left n=4 mice, right n=5 mice). Contralaterally, an optical fibre-ferrule (specifications as above) was directed into the BA. Implants were attached to the skull using two screws and dental cement. Experiments began 5 weeks after surgery.

Combined in vivo optogenetics and drug infusion: A viral vector containing Cre-dependent ChR2 or YFP was injected into the DRN of 5-HTTCre mice. Bilateral opto-fluid cannulae (5 mm long; Doric Lenses) were positioned above the BA and chronically implanted using dental cement. Experiments were conducted 5 weeks after surgery.

5-HT neuron terminal tracing: A viral vector containing Cre-dependent fluorescent synaptophysin (AAV8.2-hEF1a-DIO-synaptophysin-eYFP or AAV8.2-hEF1a-DIO-synaptophysin-mCherry) (0.6 μL, Gene Delivery Technology Core, Massachusetts General Hospital) was delivered into the DRN of either 5-HTT-Cre mice or wild-type mice injected

bilaterally in the BA with a retrograde viral vector containing Cre recombinase (retro-AAV2-Ef1a-Cre) (0.2 μL, Salk Institute Viral Vector Core) and orange dye (DiI, Thermo Fisher Scientific). Mice were perfused 5 weeks after injections.

Retrograde tracing: CTb conjugated to Alexa Fluor 555 or Alexa Fluor 488 (1 g, 0.2 μL; Invitrogen) was injected bilaterally into the BA or NA of wild-type mice. For dual CTb experiments, colours were counterbalanced across BA and NA injections (555, BA n=2 mice, NA n=3 mice; 488, BA n=3 mice, NA n=2 mice). For immunostaining experiments, 7 days later, experimental mice underwent fear conditioning (procedure as described below for fibre photometry) and controls remained in the conditioning context for the same length of time. Mice were perfused 2.5 hours later.

Identification of inputs to 5-HT neurons via cTRIO: A retrograde viral vector containing FLPo (retro-AAV2-pEF1a-DIO-FLPo-WPRE-hGHpA) (0.2 μL, Addgene, Vigene) was injected bilaterally into either the BA or NA of 5-HTT-Cre mice (together with the marker dye, DiI) (Schwarz et al., 2015). Rabies starter viruses containing FLPo-dependent rabies glycoprotein (AAV2-CAG-FLEx(FRT)-G) and the EnvA receptor TVA (AAV2-CAG-FLEx(FRT)-TC) (1.1 ratio, 0.6 μL, Addgene, Vigene) were delivered into the DRN. 4 weeks later, the retrogradely transfecting, EnvA-pseudotyped, glycoprotein gene-deleted rabies virus carrying GFP (EnvA+RVdG-eGFP) (1 μL, Salk Institute Viral Vector Core) was injected into the DRN. Mice were perfused 5 days later.

Anterograde trans-synaptic tracing: A trans-synaptic viral vector containing Cre recombinase (AAV1-hSyn-Cre-WPRE-hGH) (0.2 μL, University of Pennsylvania Vector Core) was injected into the DRN, and a Cre-dependent YFP vector (0.2 μL) was injected bilaterally into the BA of wild-type mice (Zingg et al., 2017). Mice were perfused 8 weeks later.

Fibre photometry—Prior to testing, mice were handled for 6 days and habituated to being connected to optical fibre cables in the home cage for 3 days. Before each test session, mice were acclimated to the connected cables and testing context for 10 min. The fear learning task was conducted as previously described (Bukalo et al., 2015; Gunduz-Cinar et al., 2018). On day 1, fear conditioning was conducted in a 30×25×25 cm chamber with a metal rod floor, metal walls, and a distinctive vanilla olfactory cue (context A). After 180 s acclimation, mice received 3 pairings (60 to 90 s inter-trial interval) of a 30 s, 80 dB white noise cue (CS) and a co-terminating, 0.5 s, 0.6 mA scrambled footshock (US). On day 2, fear extinction training was conducted in a different room, in a 27×27×14 cm chamber with transparent walls, a floor covered with bedding, and a distinctive acetic acid olfactory cue (context B). After 180 s acclimation, 50×30 s CS presentations (10 s inter-CS interval) were delivered. On day 3, after 180 s of acclimation, retrieval was tested in context B with 5×30 s CS presentations (10 s inter-CS interval). CS and US presentations were controlled by the Med Associates Video Freeze system (Med Associates Inc.). Freezing was defined as the absence of visible movement for at least 1 s, excluding respiration, and was scored as present or not present at 5 s intervals by an observer. For locomotion analysis, Video Freeze

software calculated a motion index (arbitrary units, a.u.) from change in video pixel composition over time.

For the discriminative fear conditioning task, day 1 consisted of a conditioning session (Context A): After 180 s acclimation, mice received 3 pairings (60 to 90 s inter-trial interval) of a 30 s, auditory cue (CS+) and a co-terminating, 0.5 s, 0.6 mA scrambled footshock. Interleaved were 3 presentations of a different auditory cue (CS−) that was not paired with a shock. CS+ and CS− assignations were counterbalanced between 80 dB white noise and a 2.9 kHz tone. On day 2, fear retrieval was tested (Context B): After 180 s of acclimation, interleaved 5×30 s CS+ and CS− presentations (10 s inter-CS interval) were delivered.

Fibre photometry recordings were made during the fear learning task to optically monitor calcium signals as a measure of neuronal activity. Fluorescence signals were recorded from DRN 5-HT projections using the Doric photometry system (Doric Lenses) (Beas et al., 2018). Continuous LED light was delivered at two wavelengths, 465 nm (LEDC1-B_FC) and 405 nm (LEDC1–405_FC), to excite GCaMP6 and an ultraviolet autofluorescence signal, respectively. LEDs were coupled to optical fibre patch cords (400 μm, 0.48 numerical aperture), which were connected to the optical fibre ferrules (400 μm) implanted in mice. The intensity of the patch cable output was between 30 and 45 W, and was kept constant for each mouse over testing sessions. GCaMP6 and autofluorescence signals were received through the same optical fibre and detected by a photoreceiver (2151, Newport Corporation). A real-time signal processor (RZ5P, Tucker-Davis Technologies) was used to sinusoidally modulate LED outputs. Data was collected at a frequency of 1017 Hz. CS presentation timings were marked by TTL input.

Optogenetics—The fear learning task was conducted as described above for fibre photometry, but with the following differences: 1) After connecting the cables to the cranial implants, mice were allowed to settle in their home cage for 10 min before testing sessions. 2) During extinction training and extinction retrieval sessions, a 5 s inter-CS interval was applied. 3) On day 4, mice were returned to Context A for 5 min. 4) Locomotor velocity was measured around the first CS-US pairing of the fear conditioning session using the Ethovision videotracking system (Noldus Information Technology Inc.) during the last 30 s of baseline, 29.5 s of pre-shock CS and light stimulation, 0.5 s of shock and light stimulation, and the first 30 s post-shock of the inter-trial interval. The experimenter was blind to mouse opsin group.

To excite or inhibit 5-HT axons in the BA, a blue laser (λ = 473 nm) was bilaterally shone onto ChR2- or iC++-transfected DRN 5-HT fibres in the BA. The power of the blue laser was adjusted to ~10 mW from the tip of the optical fibre, calculated based on the transmission efficiency of individual optical fibre-ferrules. Laser power was calibrated before testing each mouse by measuring the power at the tip of the optical fibre patch cord (125 μm, 0.22 numerical aperture) with a PM100D optical power metre with a S120C sensor (Thorlabs). Optogenetic manipulations were made throughout the duration of 30 s CS presentations continuously (for iC++), or at 20 Hz (5 ms pulses, for ChR2) to match the physiological activity of 5-HT neurons during arousal; exposure to salient stimuli elevates the firing of DRN 5-HT neurons to about 20 Hz and higher *in vivo* (Cohen et al., 2015; Li et

al., 2016). DRN 5-HT neurons transfected with Cre-dependent ChR2 in 5-HTT-Cre mice have previously been demonstrated to follow 20 Hz optical stimulation with their firing and to sustain 5-HT signalling over the course of 30 s stimulation periods *ex vivo* (Sengupta et al., 2017). In contrast, iC++ has been activated using continuous light stimulation to inhibit neuronal activity (Berndt et al., 2016). Laser stimulation was delivered in this manner during either the fear conditioning or extinction session.

In a pseudo-conditioning control experiment, fear conditioning was conducted as described above, including the 20 Hz light delivery, but in the absence of the US. Subsequent testing was restricted to a 5-CS retrieval test on day 2.

Combined in vivo optogenetics and neuronal recordings—Behavioural procedures were as above for fibre photometry, but with the following differences to accommodate the recordings: 1) After connecting the cables to their head implants, mice were allowed to settle in their home cage for 10 min before the fear conditioning session. 2) Fear conditioning was conducted in a 27 × 27 × 11 cm chamber with a metal rod floor, metal walls, and a distinctive vanilla olfactory cue (context A), and entailed 3 pairings of a 30 s, 80 dB white noise pip train (250 ms pips at 1 Hz; CS) and a co-terminating, 0.5 s, 0.6 mA scrambled footshock (US). Blue laser light was delivered at 20 Hz during the conditioning CSs, as described above for optogenetics. 3) Fear extinction training and retrieval were conducted in a 20 cm diameter Plexiglas cylinder with stripe-patterned walls and a distinctive acetic acid olfactory cue (context B). The experimenter was blind to mouse opsin group.

CS and US presentations were controlled by the Med Associates MedPC system (Med Associates Inc.). Freezing was defined as the absence of visible movement for at least 1 s, excluding respiration, and manually scored by an observer onto the CinePlex Behavioral Research System software platform (Plexon). Neural recordings were made during the fear learning task using the Omniplex Neural Data Acquisition System (Plexon).

Combined in vivo optogenetics and drug infusion—Behavioural procedures were as above for optogenetics experiments. 15 min prior to conditioning, mice received bilateral microinjections of vehicle or a drug cocktail of WAY100635 (0.37 nmol; Tocris Bioscience) and MDL100907 (0.54 nmol; Tocris Bioscience) into the BA to block 5-HT_{1A} and 5-HT_{2A} receptors, respectively (Gomes et al., 2012; Amodeo et al., 2017). Needles (6 mm) connected to a microliter syringe (2 μL, Hamilton) through a segment of polyethylene tubing were inserted into the guide cannulae. The injection needles extended 1 mm beyond the guide cannulae. The solutions were injected using an infusion pump (PHD 22/2000, Harvard Apparatus). A 0.3 L solution volume was injected over 2 min. Following injections, the needles remained in the guide cannulae for an additional 3 min to ensure diffusion into the BA and minimise reflux.

Optical fibres (5.8 mm length, 200 m diameter, 0.37 numerical aperture; Doric Lenses) connected to patch cables were inserted into the guide cannulae, extending 0.8 mm beyond the guide cannulae. Mice were acclimated to the cables for 10 min in their home cage prior

to fear conditioning. Blue laser light was delivered at 20 Hz during the conditioning CSs, as described above. The experimenter was blind to mouse opsin group and infusion compound.

Histology and immunohistochemistry—Mice were terminally overdosed with pentobarbital and transcardially perfused with PBS, followed by 4% PFA. After overnight suspension in 4% PFA at 4°C, 50 m coronal sections were cut with a vibratome (VT1000 S, Leica).

YFP and mCherry signals were amplified with immunostaining. Brain sections were incubated in blocking solution (10% normal goat serum (Vector Laboratories) and 2% bovine serum albumin (MP Biomedicals) in 0.05 M PBS with 0.3% Triton X-100) for 90 min at room temperature and then incubated at 4°C overnight in chicken anti-GFP (1:3000 dilution; 13970, Abcam) or rabbit anti-DsRed (1:200 dilution; 632496, Clontech) primary antibody to enhance visualisation of fluorescent reporters. The next day, sections were incubated in goat anti-chicken Alexa 488 (1:1000 dilution; 150169, Abcam) or goat anti-rabbit Alexa 555 (1:500 dilution; A21428, Life Technologies) secondary antibody.

For 5-HT/VGluT3/c-Fos triple-staining, brain sections were rinsed 3 times in 0.05 M PBS with 0.3% Triton X-100 (10 min), incubated in blocking solution (1% normal donkey serum (Jackson ImmunoResearch Laboratories, Inc.) and 0.1% bovine serum albumin in 0.05 M PBS) for 90 min at room temperature, and then incubated at 4°C for two nights in rabbit antic-Fos (1:250 dilution; #2250, Cell Signaling Technology), goat anti-5-HT (1:400 dilution; 20079, ImmunoStar), and guinea pig anti-VGluT3 (1:200 dilution; AB_2571855, Frontier Institute) primary antibodies. Sections were then incubated in donkey anti-rabbit Alexa 488 (1:250 dilution; A21206, Life Technologies), donkey anti-goat Alexa 350 (1:200 dilution; A21081, Life Technologies), and donkey anti-guinea pig Alexa 647 (1:200 dilution; AP193SA6, Millipore) secondary antibodies.

For DBH staining, brain sections were incubated in blocking solution (1% normal goat serum and 0.1% bovine serum albumin in 0.05 M PBS with 0.3% Triton X-100) for 90 min at room temperature and then incubated at 4°C for two nights in rabbit anti-DBH primary antibody (1:2000 dilution; #22806, Immunostar). Sections were then incubated in goat anti-rabbit Alexa 488 secondary antibody (1:250 dilution; A11034, Life Technologies).

Microscopy—All images presented were taken from coronal sections using fluorescent microscopy, unless otherwise stated. In the latter case, images were taken from sagittal sections and/or using brightfield microscopy. Placement maps and schematics were made using the Paxinos and Franklin mouse brain atlas (2001).

Images were taken to verify virus expression and implant placements using an epifluorescent BX41 microscope (Olympus), an epifluorescent BX61/VS120 slide scanner (Olympus), or a Zeiss LSM 700 confocal microscope (Carl Zeiss Microscopy). Brightfield images were taken with the BX41 microscope.

The Zeiss LSM 700 confocal microscope was used to image sections for CTb, anterograde trans-synaptic tracing, synaptophysin, and 5-HT axonal staining experiments. For synaptophysin and triple-staining CTb experiments, series of stacked images (10 m depth)

were acquired using a 20× objective lens (Plan-APOCHROMAT, 0.80 numerical aperture) with 1 m steps. For other CTb experiments, images were taken at a single optical plane through the 20× objective. For anterograde trans-synaptic tracing, images were taken through a 5× objective (FLUAR, 0.25 numerical aperture). For 5-HT axons, images were taken through a 63× oil immersion objective (Plan-APOCHROMAT, 1.40 numerical aperture).

Imaging for cTRIO experiments was conducted using the BX61/VS120 slide scanner. Tiled images were taken through a 20× objective (UPlanSApo, 0.75 numerical aperture). Representative whole-section images of synaptophysin expression were tiled using a 10× objective (UPlanSApo, 0.40 numerical aperture) on the BX61/VS120 slide scanner.

QUANTIFICATION AND STATISTICAL ANALYSIS

Behaviour—Time spent freezing was converted to a percentage ([number of freezing observations/total number of observations]×100]. The experimenter was blind to mouse opsin and infusion compound groups. For the conditioning session, freezing was analysed per CS presentation. For extinction and retrieval sessions, CS presentations were grouped into 5-trial blocks. There were no significant differences between females and males in freezing (2-way RM ANOVA; conditioning [time $F(3,18)=5.50$, $p=0.007$; sex $F(1,6)=1.47$, $p=0.271$; time×sex $F(3,18)=1.07$, $p=0.389$], extinction [time $F(10,60)=10.54$, $p<0.001$; sex $F(1,6)=0.02$, $p=0.901$; time×sex $F(10,60)=0.50$, $p=0.883$], retrieval [time $F(1,6)=37.31$, $p=0.001$; sex $F(1,6)=0.88$, $p=0.384$; time×sex $F(1,6)=1.45$, $p=0.274$]). Sample sizes (n) refer to number of mice per group and are detailed in the figure legends.

In vivo fibre photometry—Recordings were made from the ultraviolet channel to control for changes in autofluorescence, bleaching, and motion artefacts in the GCaMP6 signal. Specifically, the ultraviolet signal was aligned to the GCaMP6 signal by linear fitting. The GCaMP6 signal was then normalised to the fitted control, by calculating change in fluorescence (F = GCaMP6 signal – fitted ultraviolet signal) and dividing by the fitted ultraviolet signal at the same time point (F/F, dF/F). Z-score transformations of dF/F were made by normalising to baseline, which was taken over the 180 s before CS onset. Changes in dF/F were considered significant only if they were at least 1.96 s.d. above or below baseline signal ($\alpha=0.05$). Z-scored traces were exponentially smoothed by a damping factor of 0.9 for graphical presentation. Area under the curve calculations were performed on z-scored dF/F traces. There were no significant differences between females and males in area under the curve values for BA 5-HT projection function (2-way RM ANOVA; conditioning [time $F(8,40)=13.83$, $p<0.001$; sex $F(1,5)=2.90$, $p=0.149$; time×sex $F(8,40)=0.98$, $p=0.465$] extinction [time $F(2,6)=5.20$, $p=0.049$; sex $F(1,3)=0.09$, $p=0.780$; time×sex $F(2,6)=0.22$, $p=0.808$] retrieval [time $F(1,6)=1.64$, $p=0.248$; sex $F(1,6)=0.29$, $p=0.612$; time×sex $F(1,6)=0.29$, $p=0.612$). Sample sizes (n) refer to number of mice per group and are detailed in the figure legends and Results section.

In vivo electrophysiological recordings—BA single units were sorted and waveforms isolated manually using principal component analysis on Offline Sorter software (Plexon). Spikes were included in analyses if they displayed a refractory period of at least 1 ms.

Autocorrelograms from simultaneously recorded units were compared to ensure that cells were not counted twice. Data from the 0.5 s during US delivery at the end of the conditioning CSs were excluded due to electrical noise. Units firing less than 10 times during CS presentations were excluded. Single units were analysed by generating perievent histograms of firing rates with 0.01 s bins for CS-pips. Firing rates were considered from 250 ms before pip onset until 250 ms after pip offset using NeuroExplorer (Nex Technologies). Z-score transformations of firing rates were made by normalising to baseline, which was taken over the 250 ms before CS-pip onset. Firing rate responses were considered significant only if they were at least 2.58 s.d. above or below baseline firing rates for two consecutive time bins. The 2-tailed alpha value (α=0.01) and corresponding s.d. cut-offs were chosen based on the perievent histogram bins (Halladay and Blair, 2015). Sample sizes (n) refer to number of recorded units and mice per group, and are detailed in the figure legends.

Over the course of the first 5 extinction CS presentations, changes in single unit activity patterns were examined. A unit was considered to become increasingly excited if it was excited during CS-pips only after the second CS. A unit was considered to become decreasingly excited if it stopped being excited only after the second CS. A unit was considered consistently excited if it was excited during at least 4 of the CS presentations, including the first and last.

Local field potentials were low-pass filtered offline up to 20 Hz. Perievent spectrograms and power spectral densities of continuous data were generated using fourier transform analyses on NeuroExplorer. Power spectra were calculated for individual CS presentations (conditioning) or averaged over 5-CS blocks (extinction training and retrieval). Power spectra were normalised and expressed for each frequency bin as a percentage of the total power between 0 and 20 Hz. In particular, delta (1–4 Hz), theta (4–9 Hz), alpha (9–14 Hz), and beta (14–20 Hz) oscillations were considered (Barkus et al., 2014). As a control measure, the power spectral density of local field potentials for the last 30 s of the extinction baseline period was calculated to assess whether baseline network oscillations were altered by optogenetic manipulation after fear conditioning.

For correlations, leverage analysis was conducted using MATLAB (MathWorks, Inc.). Values with Cook's distance (D_i) values greater than 1 were excluded as influential outliers (YFP n=1 mouse, ChR2 n=1 mouse).

For phase-locking analysis, local field potentials were Hann filtered for the theta range (4–9 Hz) and the Hilbert transformation was used to convert to theta phase with NeuroExplorer. The Circular Statistics Toolbox (Directional Statistics) by Philipp Berens and custom code were used to assess phase-locking of single unit firing with the Rayleigh test (p values<0.05 were considered significantly phase-locked) on MATLAB. Units firing less than 10 times during the analysed CS presentations were excluded.

Cell counting—For CTb experiments, images were taken from 5 alternating DRN sections per mouse brain (rostro-caudal coordinates approximately −4.3 to −4.9 mm from bregma). Counting was performed using Zen lite software (Carl Zeiss Microscopy). For cTRIO

experiments, images were taken from 1 per 3 brain sections (excluding from approximately 0.0 to −1.0 from bregma, where brains were mounted for sectioning). Counting was performed using OlyVIA (Olympus) and FIJI (Image J) software (Schindelin et al., 2012). The experimenter was blind to target pathway and behavioural exposure groups. Sample sizes (n) refer to number of counted cells and mice per group, and are detailed in the figure legends and Results section.

Fluorescence intensity quantification—For synaptophysin and anterograde trans-synaptic tracing experiments, images were taken using the same acquisition parameters for each experiment. Images were taken from 1 per 3 brain sections (excluding from approximately 0.0 to −1.0 from bregma, where brains were mounted for sectioning). Mean intensity of fluorescence was quantified using FIJI software. Sample sizes (n) refer to number of mice per group and are detailed in the figure legends.

Statistical tests—Behavioural, photometric, electrophysiological, and immunohistochemical data were analysed using RM (repeated measures) ANOVA and Sidak multiple comparison tests (when main effects for 1-way or interactions for 2- and 3-way analyses were significant). T-tests were used without corrections across separate datasets when the Shapiro-Wilk normality test was passed; otherwise, Mann Whitney or Wilcoxon signed-rank tests were used.

The strength of relationships between behavioural and photometric or electrophysiological measurements was evaluated using Pearson's correlation. For electrophysiology data, proportions of single units were compared with Fisher's exact or chi-square tests. Single unit periodicity was assessed with the Rayleigh test. CTb data were analysed using 1-sample t-tests. Synaptophysin and cTRIO data were analysed with t-tests.

Data were processed on Excel (Microsoft Corporation). Statistical tests were conducted using GraphPad Prism (GraphPad Software, Inc.), SPSS (IBM), or MATLAB software. Statistics are reported in the Results section.

Supplementary Material

Refer to Web version on PubMed Central for supplementary material.

Acknowledgements

Research was funded by the NIAAA IRP. We thank Dr. O. Bukalo, Dr. M. Penzo, N. Ringelberg, Dr. M. Krashes, and J. Liang for sharing technical expertise in fibre photometry, Dr. A.M. Bygrave for custom Matlab code, and, for training and critical advice, Drs. M.Nonaka (microscopy), L.R. Halladay (electrophysiology), O. Gunduz-Cinar (pharmacology), and O. Bukalo (optogenetics). We also thank J. Schaffer for help managing mouse colonies, Dr. T. Kash for sharing 5-HTT-Cre mice, and Dr. D. Lovinger for sharing GAD2-IRES-Cre mice. We thank Drs. G. Schoenbaum, J. Cohen, and D. Bannerman for helpful discussions, and Drs. M. Penzo, M. Krashes, and A.M. Bygrave for valuable comments on an earlier version of the manuscript.

References

Akirav I, Raizel H, and Maroun M (2006). Enhancement of conditioned fear extinction by infusion of the GABA A agonist muscimol into the rat prefrontal cortex and amygdala. Eur. J. Neurosci 23, 758–764. [PubMed: 16487156]

Allers KA, and Sharp T (2003). Neurochemical and anatomical identification of fast- and slow-firing neurones in the rat dorsal raphe nucleus using juxtacellular labelling methods in vivo. Neuroscience 122, 193–204. [PubMed: 14596860]

Amilhon B, Lepicard E, Renoir T, Mongeau R, Popa D, Poirel O, Miot S, Gras C, Gardier AM, Gallego J, et al. (2010). VGLUT3 (Vesicular Glutamate Transporter Type 3) Contribution to the Regulation of Serotonergic Transmission and Anxiety. J. Neurosci 30, 2198–2210. [PubMed: 20147547]

Anglada-Figueroa D, and Quirk G (2005). Lesions of the Basal Amygdala Block Expression of Conditioned Fear But Not Extinction. J. Neurosci 25, 9680–9685. [PubMed: 16237172]

Ansorge MS, Zhou M, Lira A, Hen R, and Gingrich JA (2004). Early-life blockade of the 5-HT transporter alters emotional behavior in adult mice. Science (80-.) 306, 879–881.

Bang SJ, Jensen P, Dymecki SM, and Commons KG (2012). Projections and interconnections of genetically defined serotonin neurons in mice. Eur. J. Neurosci 35, 85–96. [PubMed: 22151329]

Baratta MV, Kodandaramaiah SB, Monahan PE, Yao J, Weber MD, Lin P-A, Gisabella B, Petrossian N, Amat J, Kim K, et al. (2016). Stress Enables Reinforcement-Elicited Serotonergic Consolidation of Fear Memory. Biol. Psychiatry 79, 814–822. [PubMed: 26248536]

Barkus C, Line SJ, Huber A, Capitao L, Lima J, Jennings K, Lowry J, Sharp T, Bannerman DM, and McHugh SB (2014). Variation in Serotonin Transporter Expression Modulates Fear-Evoked Hemodynamic Responses and Theta-Frequency Neuronal Oscillations in the Amygdala. Biol. Psychiatry 75, 901–908. [PubMed: 24120093]

Barnes NM, and Sharp T (1999). A review of central 5-HT receptors and their function. Neuropharmacology 38, 1083–1152. [PubMed: 10462127]

Bazelot M, Bocchio M, Kasugai Y, Fischer D, Dodson PD, Ferraguti F, and Capogna M (2015). Hippocampal Theta Input to the Amygdala Shapes Feedforward Inhibition to Gate Heterosynaptic Plasticity. Neuron 87, 1290–1303. [PubMed: 26402610]

Beas BS, Wright BJ, Skirzewski M, Leng Y, Hyun JH, Koita O, Ringelberg N, Kwon H-B, Buonanno A, and Penzo MA (2018). The locus coeruleus drives disinhibition in the midline thalamus via a dopaminergic mechanism. Nat. Neurosci 21, 963–973. [PubMed: 29915192]

Belmer A, Klenowski PM, Patkar OL, and Bartlett SE (2017). Mapping the connectivity of serotonin transporter immunoreactive axons to excitatory and inhibitory neurochemical synapses in the mouse limbic brain. Brain Struct. Funct 222, 1297–1314. [PubMed: 27485750]

Berndt A, Lee SY, Wietek J, Ramakrishnan C, Steinberg EE, Rashid AJ, Kim H, Park S, Santoro A, Frankland PW, et al. (2016). Structural foundations of optogenetics: Determinants of channelrhodopsin ion selectivity. Proc. Natl. Acad. Sci. U. S. A 113, 822–829. [PubMed: 26699459]

Bocchio M, Fucsina G, Oikonomidis L, McHugh SB, Bannerman DM, Sharp T, and Capogna M (2015). Increased Serotonin Transporter Expression Reduces Fear and Recruitment of Parvalbumin Interneurons of the Amygdala. Neuropsychopharmacology 40, 3015–3026. [PubMed: 26052039]

Bocchio M, McHugh SB, Bannerman DM, Sharp T, and Capogna M (2016). Serotonin, Amygdala and Fear: Assembling the Puzzle. Front. Neural Circuits 10, 24. [PubMed: 27092057]

Bocchio M, Nabavi S, and Capogna M (2017). Synaptic Plasticity, Engrams, and Network Oscillations in Amygdala Circuits for Storage and Retrieval of Emotional Memories. Neuron 94, 731–743. [PubMed: 28521127]

Bosker FJ, Cremers TIFH, Jongsma ME, Westerink BHC, Wikström HV, and Den Boer JA (2001). Acute and chronic effects of citalopram on postsynaptic 5-hydroxytryptamine1A receptor-mediated feedback: A microdialysis study in the amygdala. J. Neurochem 76, 1645–1653. [PubMed: 11259482]

Bukalo O, Pinard CR, Silverstein S, Brehm C, Hartley ND, Whittle N, Colacicco G, Busch E, Patel S, Singewald N, et al. (2015). Prefrontal inputs to the amygdala instruct fear extinction memory formation. Sci. Adv 1, e1500251–e1500251. [PubMed: 26504902]

Burghardt NS, Sullivan GM, McEwen BS, Gorman JM, and LeDoux JE (2004). The selective serotonin reuptake inhibitor citalopram increases fear after acute treatment but reduces fear with chronic treatment: a comparison with tianeptine. Biol. Psychiatry 55, 1171–1178. [PubMed: 15184036]

Calizo LH, Akanwa A, Ma X, Pan Y, Lemos JC, Craige C, Heemstra LA, and Beck SG (2011). Raphe serotonin neurons are not homogenous: Electrophysiological, morphological and neurochemical evidence. Neuropharmacology 61, 524–543. [PubMed: 21530552]

Caspi A, Hariri AR, Holmes A, Uher R, and Moffitt TE (2010). Genetic Sensitivity to the Environment: The Case of the Serotonin Transporter Gene and Its Implications for Studying Complex Diseases and Traits. Am. J. Psychiatry 167, 509–527. [PubMed: 20231323]

Chen A, Hough CJ, and Li H (2003). Serotonin type II receptor activation facilitates synaptic plasticity via n-methyl-d-aspartate-mediated mechanism in the rat basolateral amygdala. Neuroscience 119, 53–63. [PubMed: 12763068]

Cheng L, Wang S, and Gean P (1998). Serotonin depresses excitatory synaptic transmission and depolarization-evoked Ca 2+ influx in rat basolateral amygdala via 5-HT 1A receptors. Eur. J. Neurosci 10, 2163–2172. [PubMed: 9753102]

Christianson JP, Ragole T, Amat J, Greenwood BN, Strong PV, Paul ED, Fleshner M, Watkins LR, and Maier SF (2010). 5-Hydroxytryptamine 2C Receptors in the Basolateral Amygdala Are Involved in the Expression of Anxiety After Uncontrollable Traumatic Stress. Biol. Psychiatry 67, 339–345. [PubMed: 19914601]

Cohen JY, Amoroso MW, and Uchida N (2015). Serotonergic neurons signal reward and punishment on multiple timescales. Elife 4, 1–25.

Cornélio AM, and Nunes-de-Souza RL (2007). Anxiogenic-like effects of mCPP microinfusions into the amygdala (but not dorsal or ventral hippocampus) in mice exposed to elevated plus-maze. Behav. Brain Res 178, 82–89. [PubMed: 17207863]

Correia PA, Lottem E, Banerjee D, Machado AS, Carey MR, and Mainen ZF (2017). Transient inhibition and long-term facilitation of locomotion by phasic optogenetic activation of serotonin neurons. Elife 6, 1–27.

Davis P, Zaki Y, Maguire J, and Reijmers LG (2017). Cellular and oscillatory substrates of fear extinction learning. Nat. Neurosci 20, 1624–1633. [PubMed: 28967909]

Deneris E, and Gaspar P (2018). Serotonin neuron development: shaping molecular and structural identities. Wiley Interdiscip. Rev. Dev. Biol 7, e301.

Fernandez SP, Cauli B, Cabezas C, Muzerelle A, Poncer J-C, and Gaspar P (2016). Multiscale single-cell analysis reveals unique phenotypes of raphe 5-HT neurons projecting to the forebrain. Brain Struct. Funct 221, 4007–4025. [PubMed: 26608830]

Fu W, Le Maître E, Fabre V, Bernard J-F, David Xu Z-Q, and Hökfelt T (2010). Chemical neuroanatomy of the dorsal raphe nucleus and adjacent structures of the mouse brain. J. Comp. Neurol 518, 3464–3494. [PubMed: 20589909]

Gagnon D, and Parent M (2014). Distribution of VGLUT3 in Highly Collateralized Axons from the Rat Dorsal Raphe Nucleus as Revealed by Single-Neuron Reconstructions. PLoS One 9, e87709. [PubMed: 24504335]

Graeff FG, Guimarães FS, De Andrade TGCS, and Deakin JFW (1996). Role of 5-HT in stress, anxiety, and depression. Pharmacol. Biochem. Behav 54, 129–141. [PubMed: 8728550]

Grahn R., Will M, Hammack S., Maswood S, McQueen M., Watkins L., and Maier S. (1999). Activation of serotonin-immunoreactive cells in the dorsal raphe nucleus in rats exposed to an uncontrollable stressor. Brain Res 826, 35–43. [PubMed: 10216194]

Gunduz-Cinar O, Brockway E, Lederle L, Wilcox T, Halladay LR, Ding Y, Oh H, Busch EF, Kaugars K, Flynn S, et al. (2018). Identification of a novel gene regulating amygdala-mediated fear extinction. Mol. Psychiatry

Guo J-D, O'Flaherty BM, and Rainnie DG (2017). Serotonin gating of cortical and thalamic glutamate inputs onto principal neurons of the basolateral amygdala. Neuropharmacology 126, 224–232. [PubMed: 28899729]

Hajós M, Allers KA, Jennings K, Sharp T, Charette G, Sík A, and Kocsis B (2007). Neurochemical identification of stereotypic burst-firing neurons in the rat dorsal raphe nucleus using juxtacellular labelling methods. Eur. J. Neurosci 25, 119–126. [PubMed: 17241273]

Hale MW, and Lowry CA (2011). Functional topography of midbrain and pontine serotonergic systems: implications for synaptic regulation of serotonergic circuits. Psychopharmacology (Berl) 213, 243–264. [PubMed: 21088958]

Halladay LR, and Blair HT (2015). Distinct ensembles of medial prefrontal cortex neurons are activated by threatening stimuli that elicit excitation vs. inhibition of movement. J. Neurophysiol 114, 793–807. [PubMed: 25972588]

Herry C, and Johansen JP (2014). Encoding of fear learning and memory in distributed neuronal circuits. Nat. Neurosci 17, 1644–1654. [PubMed: 25413091]

Herry C, Ciocchi S, Senn V, Demmou L, Müller C, and Lüthi A (2008). Switching on and off fear by distinct neuronal circuits. Nature 454, 600–606. [PubMed: 18615015]

Holmes A (2008). Genetic variation in cortico-amygdala serotonin function and risk for stress-related disease. Neurosci. Biobehav. Rev 32, 1293–1314. [PubMed: 18439676]

Holmes A, Yang RJ, Lesch K-P, Crawley JN, and Murphy DL (2003). Mice lacking the serotonin transporter exhibit 5-HT(1A) receptor-mediated abnormalities in tests for anxiety-like behavior. Neuropsychopharmacology 28, 2077–2088. [PubMed: 12968128]

Homberg JR, and Lesch K-P (2011). Looking on the Bright Side of Serotonin Transporter Gene Variation. Biol. Psychiatry 69, 513–519. [PubMed: 21047622]

Inoue T, Li XB, Abekawa T, Kitaichi Y, Izumi T, Nakagawa S, and Koyama T (2004). Selective serotonin reuptake inhibitor reduces conditioned fear through its effect in the amygdala. Eur. J. Pharmacol 497, 311–316. [PubMed: 15336949]

Izumi T, Ohmura Y, Futami Y, Matsuzaki H, Kubo Y, Yoshida T, and Yoshioka M (2012). Effects of serotonergic terminal lesion in the amygdala on conditioned fear and innate fear in rats. Eur. J. Pharmacol 696, 89–95. [PubMed: 23036373]

Jiang X, Xing G, Yang C, Verma A, Zhang L, and Li H (2009). Stress Impairs 5-HT2A Receptor-Mediated Serotonergic Facilitation of GABA Release in Juvenile Rat Basolateral Amygdala. Neuropsychopharmacology 34, 410–423. [PubMed: 18536707]

Johansen JP, Tarpley JW, LeDoux JE, and Blair HT (2010). Neural substrates for expectation-modulated fear learning in the amygdala and periaqueductal gray. Nat. Neurosci 13, 979–986. [PubMed: 20601946]

Johnson MD (1994). Synaptic glutamate release by postnatal rat serotonergic neurons in microculture. Neuron 12, 433–442. [PubMed: 7906530]

Johnson PL, Molosh A, Fitz SD, Arendt D, Deehan GA, Federici LM, Bernabe C, Engleman EA, Rodd ZA, Lowry CA, et al. (2015). Pharmacological depletion of serotonin in the basolateral amygdala complex reduces anxiety and disrupts fear conditioning. Pharmacol. Biochem. Behav 138, 174–179. [PubMed: 26476009]

Karalis N, Dejean C, Chaudun F, Khoder S, Rozeske RR, Wurtz H, Bagur S, Benchenane K, Sirota A, Courtin J, et al. (2016). 4-Hz oscillations synchronize prefrontal–amygdala circuits during fear behavior. Nat. Neurosci 19, 605–612. [PubMed: 26878674]

Kocsis B, Varga V, Dahan L, and Sik A (2006). Serotonergic neuron diversity: Identification of raphe neurons with discharges time-locked to the hippocampal theta rhythm. Proc. Natl. Acad. Sci 103, 1059–1064. [PubMed: 16418294]

LeDoux JE (2014). Coming to terms with fear. Proc. Natl. Acad. Sci. U. S. A 111, 2871–2878. [PubMed: 24501122]

Li X, Inoue T, Abekawa T, Weng S, Nakagawa S, Izumi T, and Koyama T (2006). 5-HT1A receptor agonist affects fear conditioning through stimulations of the postsynaptic 5-HT1A receptors in the hippocampus and amygdala. Eur. J. Pharmacol 532, 74–80. [PubMed: 16460727]

Li Y, Zhong W, Wang D, Feng Q, Liu Z, Zhou J, Jia C, Hu F, Zeng J, Guo Q, et al. (2016). Serotonin neurons in the dorsal raphe nucleus encode reward signals. Nat. Commun 7, 10503. [PubMed: 26818705]

Liang KC (1999). Pre- or post-training injection of buspirone impaired retention in the inhibitory avoidance task: involvement of amygdala 5-HT 1A receptors. Eur. J. Neurosci 11, 1491–1500. [PubMed: 10215901]

Likhtik E, Stujenske JM, A Topiwala M, Harris AZ, and Gordon JA (2014). Prefrontal entrainment of amygdala activity signals safety in learned fear and innate anxiety. Nat. Neurosci 17, 106–113. [PubMed: 24241397]

Line SJ, Barkus C, Coyle C, Jennings KA, Deacon RM, Lesch KP, Sharp T, and Bannerman DM (2011). Opposing alterations in anxiety and species-typical behaviours in serotonin transporter

overexpressor and knockout mice. Eur. Neuropsychopharmacol 21, 108–116. [PubMed: 20863670]

Line SJ, Barkus C, Rawlings N, Jennings K, Mchugh S, Sharp T, and Bannerman DM (2014). Reduced sensitivity to both positive and negative reinforcement in mice over-expressing the 5-hydroxytryptamine transporter. Eur. J. Neurosci 40, 3735–3745. [PubMed: 25283165]

Liu Z, Zhou J, Li Y, Hu F, Lu Y, Ma M, Feng Q, Zhang J, Wang D, Zeng J, et al. (2014). Dorsal Raphe Neurons Signal Reward through 5-HT and Glutamate. Neuron 81, 1360–1374. [PubMed: 24656254]

Lopreato GF, Phelan R, Borghese CM, Beckstead MJ, and Mihic SJ (2003). Inhaled drugs of abuse enhance serotonin-3 receptor function. Drug Alcohol Depend 70, 11–15. [PubMed: 12681521]

Ma QP, Yin GF, Ai MK, and Han JS (1991). Serotonergic projections from the nucleus raphe dorsalis to the amygdala in the rat. Neurosci. Lett 134, 21–24. [PubMed: 1815148]

Macedo CE, Martinez RCR, Albrechet-Souza L, Molina VA, and Brandão ML (2007). 5-HT2- and D1-mechanisms of the basolateral nucleus of the amygdala enhance conditioned fear and impair unconditioned fear. Behav. Brain Res 177, 100–108. [PubMed: 17126419]

Machado-Vieira R, Baumann J, Wheeler-Castillo C, Latov D, Henter ID, Salvadore G, and Zarate CA (2010). The Timing of Antidepressant Effects: A Comparison of Diverse Pharmacological and Somatic Treatments. Pharmaceuticals (Basel) 3, 19–41. [PubMed: 27713241]

Marcinkiewcz CA, Mazzone CM, D'Agostino G, Halladay LR, Hardaway JA, DiBerto JF, Navarro M, Burnham N, Cristiano C, Dorrier CE, et al. (2016). Serotonin engages an anxiety and fear-promoting circuit in the extended amygdala. Nature 537, 97–101. [PubMed: 27556938]

Matias S, Lottem E, Dugué GP, and Mainen ZF (2017). Activity patterns of serotonin neurons underlying cognitive flexibility. Elife 6, 1–24.

Matsuzaki H, Izumi T, Horinouchi T, Boku S, Inoue T, Yamaguchi T, Yoshida T, Matsumoto M, Togashi H, Miwa S, et al. (2011). Juvenile stress attenuates the dorsal hippocampal postsynaptic 5-HT1A receptor function in adult rats. Psychopharmacology (Berl) 214, 329–337. [PubMed: 20714708]

McCall JG, Siuda ER, Bhatti DL, Lawson LA, McElligott ZA, Stuber GD, and Bruchas MR (2017). Locus coeruleus to basolateral amygdala noradrenergic projections promote anxiety-like behavior. Elife 6, 1–23.

McHugh SB, Barkus C, Huber A, Capitao L, Lima J, Lowry JP, and Bannerman DM (2014). Aversive Prediction Error Signals in the Amygdala. J. Neurosci 34, 9024–9033. [PubMed: 24990922]

Milad MR, and Quirk GJ (2012). Fear Extinction as a Model for Translational Neuroscience: Ten Years of Progress. Annu. Rev. Psychol 63, 129–151. [PubMed: 22129456]

Muller JF, Mascagni F, and McDonald AJ (2007). Serotonin-immunoreactive axon terminals innervate pyramidal cells and interneurons in the rat basolateral amygdala. J. Comp. Neurol 505, 314–335. [PubMed: 17879281]

Nagatsu I, Inagaki S, Kondo Y, Karasawa N, and Nagatsu T (1979). Immunofluorescent studies on the localization of tyrosine hydroxylase and dopamine-β-hydroxylase in the mes-, di-, and telencephalon of the rat using unperfused fresh frozen sections. Acta Histochem. Cytochem 12, 20–37.

Namburi P, Beyeler A, Yorozu S, Calhoon GG, Halbert SA, Wichmann R, Holden SS, Mertens KL, Anahtar M, Felix-Ortiz AC, et al. (2015). A circuit mechanism for differentiating positive and negative associations. Nature 520, 675–678. [PubMed: 25925480]

Narayanan V, Heiming RS, Jansen F, Lesting J, Sachser N, Pape H-C, and Seidenbecher T (2011). Social Defeat: Impact on Fear Extinction and Amygdala-Prefrontal Cortical Theta Synchrony in 5-HTT Deficient Mice. PLoS One 6, e22600. [PubMed: 21818344]

Nemeroff CB, and Owens MJ (2002). Treatment of mood disorders. Nat Neurosci 5, 1068–1070. [PubMed: 12403988]

Nonkes LJP, de Pooter M, and Homberg JR (2012). Behavioural therapy based on distraction alleviates impaired fear extinction in male serotonin transporter knockout rats. J. Psychiatry Neurosci 37, 224–230. [PubMed: 22353635]

Ogawa SK, Cohen JY, Hwang D, Uchida N, and Watabe-Uchida M (2014). Organization of Monosynaptic Inputs to the Serotonin and Dopamine Neuromodulatory Systems. Cell Rep 8, 1105–1118. [PubMed: 25108805]

Pape H-C, and Driesang RB (1998). Ionic Mechanisms of Intrinsic Oscillations in Neurons of the Basolateral Amygdaloid Complex. J. Neurophysiol 79, 217–226. [PubMed: 9425193]

Pape H-C, and Pare D (2010). Plastic Synaptic Networks of the Amygdala for the Acquisition, Expression, and Extinction of Conditioned Fear. Physiol. Rev 90, 419–463. [PubMed: 20393190]

Parsons RG, and Ressler KJ (2013). Implications of memory modulation for post-traumatic stress and fear disorders. Nat. Neurosci 16, 146–153. [PubMed: 23354388]

Pollak Dorocic I, Fürth D, Xuan Y, Johansson Y, Pozzi L, Silberberg G, Carlén M, and Meletis K (2014). A Whole-Brain Atlas of Inputs to Serotonergic Neurons of the Dorsal and Median Raphe Nuclei. Neuron 83, 663–678. [PubMed: 25102561]

Rainnie DG (1999). Serotonergic modulation of neurotransmission in the rat basolateral amygdala. J. Neurophysiol 82, 69–85. [PubMed: 10400936]

Rajmohan V, and Mohandas E (2007). The limbic system. Indian J. Psychiatry 49, 132. [PubMed: 20711399]

Rebello TJ, Yu Q, Goodfellow NM, Caffrey Cagliostro MK, Teissier A, Morelli E, Demireva EY, Chemiakine A, Rosoklija GB, Dwork AJ, et al. (2014). Postnatal day 2 to 11 constitutes a 5-HT-sensitive period impacting adult mPFC function. J. Neurosci 34, 12379–12393. [PubMed: 25209278]

Ren J, Friedmann D, Xiong J, Liu CD, Ferguson BR, Weerakkody T, DeLoach KE, Ran C, Pun A, Sun Y, et al. (2018). Anatomically Defined and Functionally Distinct Dorsal Raphe Serotonin Sub-systems. Cell

Richard JM, Ambroggi F, Janak PH, and Fields HL (2016). Ventral Pallidum Neurons Encode Incentive Value and Promote Cue-Elicited Instrumental Actions. Neuron 90, 1165–1173. [PubMed: 27238868]

Sakai K (2011). Sleep-waking discharge profiles of dorsal raphe nucleus neurons in mice. Neuroscience 197, 200–224. [PubMed: 21958868]

Sakai K, and Crochet S (2001). Differentiation of presumed serotonergic dorsal raphe neurons in relation to behavior and wake–sleep states. Neuroscience 104, 1141–1155. [PubMed: 11457597]

Schindelin J, Arganda-Carreras I, Frise E, Kaynig V, Longair M, Pietzsch T, Preibisch S, Rueden C, Saalfeld S, Schmid B, et al. (2012). Fiji: an open-source platform for biological-image analysis. Nat. Methods 9, 676–682. [PubMed: 22743772]

Schwarz LA, Miyamichi K, Gao XJ, Beier KT, Weissbourd B, DeLoach KE, Ren J, Ibanes S, Malenka RC, Kremer EJ, et al. (2015). Viral-genetic tracing of the input–output organization of a central noradrenaline circuit. Nature 524, 88–92. [PubMed: 26131933]

Schweimer JV, and Ungless MA (2010). Phasic responses in dorsal raphe serotonin neurons to noxious stimuli. Neuroscience 171, 1209–1215. [PubMed: 20888395]

Seidenbecher T (2003). Amygdalar and Hippocampal Theta Rhythm Synchronization During Fear Memory Retrieval. Science (80-.) 301, 846–850.

Sengupta A, Bocchio M, Bannerman DM, Sharp T, and Capogna M (2017). Control of Amygdala Circuits by 5-HT Neurons via 5-HT and Glutamate Cotransmission. J. Neurosci 37, 1785–1796. [PubMed: 28087766]

Senn V, Wolff SBE, Herry C, Grenier F, Ehrlich I, Gründemann J, Fadok JP, Müller C, Letzkus JJ, and Lüthi A (2014). Long-Range Connectivity Defines Behavioral Specificity of Amygdala Neurons. Neuron 81, 428–437. [PubMed: 24462103]

Seo C, Guru A, Jin M, Ito B, Sleezer BJ, Ho Y, Wang E, Boada C, Krupa NA, Kullakanda DS, et al. (2019). Intense threat switches dorsal raphe serotonin neurons to a paradoxical operational mode. Science (80-.) 363, 538–542.

Sierra-Mercado D, Padilla-Coreano N, and Quirk GJ (2011). Dissociable Roles of Prelimbic and Infralimbic Cortices, Ventral Hippocampus, and Basolateral Amygdala in the Expression and Extinction of Conditioned Fear. Neuropsychopharmacology 36, 529–538. [PubMed: 20962768]

Smith GS, Lotrich FE, Malhotra AK, Lee AT, Ma Y, Kramer E, Gregersen PK, Eidelberg D, and Pollock BG (2004). Effects of serotonin transporter promoter polymorphisms on serotonin function. Neuropsychopharmacology 29, 2226–2234. [PubMed: 15354180]

Spannuth BM, Hale MW, Evans AK, Lukkes JL, Campeau S, and Lowry CA (2011). Investigation of a central nucleus of the amygdala/dorsal raphe nucleus serotonergic circuit implicated in fear-potentiated startle. Neuroscience 179, 104–119. [PubMed: 21277950]

Steinbusch H (1981). Distribution of serotonin-immunoreactivity in the central nervous system of the rat—cell bodies and terminals. Neuroscience 6, 557–618. [PubMed: 7017455]

Takase LF, Nogueira MI, Baratta M, Bland ST, Watkins LR, Maier SF, Fornal CA, and Jacobs BL (2004). Inescapable shock activates serotonergic neurons in all raphe nuclei of rat. Behav. Brain Res 153, 233–239. [PubMed: 15219724]

Teissier A, Chemiakine A, Inbar B, Bagchi S, Ray RS, Palmiter RD, Dymecki SM, Moore H, and Ansorge MS (2015). Activity of Raphé Serotonergic Neurons Controls Emotional Behaviors. Cell Rep 13, 1965–1976. [PubMed: 26655908]

Teixeira CM, Rosen ZB, Suri D, Sun Q, Hersh M, Sargin D, Dincheva I, Morgan AA, Spivack S, Krok AC, et al. (2018). Hippocampal 5-HT Input Regulates Memory Formation and Schaffer Collateral Excitation. Neuron 98, 992–1004.e4. [PubMed: 29754752]

Tovote P, Fadok JP, and Lüthi A (2015). Neuronal circuits for fear and anxiety. Nat. Rev. Neurosci 16, 317–331. [PubMed: 25991441]

Varga V, Losonczy A, Zemelman BV, Borhegyi Z, Nyiri G, Domonkos A, Hangya B, Holderith N, Magee JC, and Freund TF (2009). Fast Synaptic Subcortical Control of Hippocampal Circuits. Science (80-.) 326, 449–453.

Vasa RA, Carlino AR, and Pine DS (2006). Pharmacotherapy of Depressed Children and Adolescents: Current Issues and Potential Directions. Biol. Psychiatry 59, 1021–1028. [PubMed: 16406250]

Vasudeva RK, Lin RCS, Simpson KL, and Waterhouse BD (2011). Functional organization of the dorsal raphe efferent system with special consideration of nitrergic cell groups. J. Chem. Neuroanat 41, 281–293. [PubMed: 21640185]

Wang H-L, Zhang S, Qi J, Wang H, Cachope R, Mejias-Aponte CA, Gomez JA, Mateo-Semidey GE, Beaudoin GMJ, Paladini CA, et al. (2019). Dorsal Raphe Dual Serotonin-Glutamate Neurons Drive Reward by Establishing Excitatory Synapses on VTA Mesoaccumbens Dopamine Neurons. Cell Rep 26, 1128–1142.e7. [PubMed: 30699344]

Weissbourd B, Ren J, DeLoach KE, Guenthner CJ, Miyamichi K, and Luo L (2014). Presynaptic Partners of Dorsal Raphe Serotonergic and GABAergic Neurons. Neuron 83, 645–662. [PubMed: 25102560]

Weisstaub NV, Zhou M, Lira A, Lambe E, González-Maeso J, Hornung J-P, Sibille E, Underwood M, Itohara S, Dauer WT, et al. (2006). Cortical 5-HT2A receptor signaling modulates anxiety-like behaviors in mice. Science 313, 536–540. [PubMed: 16873667]

Yamamoto R, Ueta Y, Sugai T, and Kato N (2012). A serotonergic discrimination favoring synaptic inputs that accompany robust spike firing in lateral amygdala neurons. Neuroscience 220, 119–130. [PubMed: 22698688]

Zhuang X, Gross C, Santarelli L, Compan V, Trillat AC, and Hen R (1999). Altered emotional states in knockout mice lacking 5-HT1A or 5-HT1B receptors. Neuropsychopharmacology 21, 52S–60S. [PubMed: 10432489]

Zingg B, Chou X, Zhang Z, Mesik L, Liang F, Tao HW, and Zhang LI (2017). AAV-Mediated Anterograde Transsynaptic Tagging: Mapping Corticocollicular Input-Defined Neural Pathways for Defense Behaviors. Neuron 93, 33–47. [PubMed: 27989459]

Highlights

- Fear learning selectively engages the anatomically distinct DRN→BA 5-HT pathway
- The DRN→BA 5-HT pathway bidirectionally modulates fear learning and extinction
- The DRN→BA 5-HT pathway sculpts fear-associated neuronal activity in the BA
- The DRN→BA 5-HT pathway expresses VGluT3 but drives fear via BA 5-HT1A/2A receptors

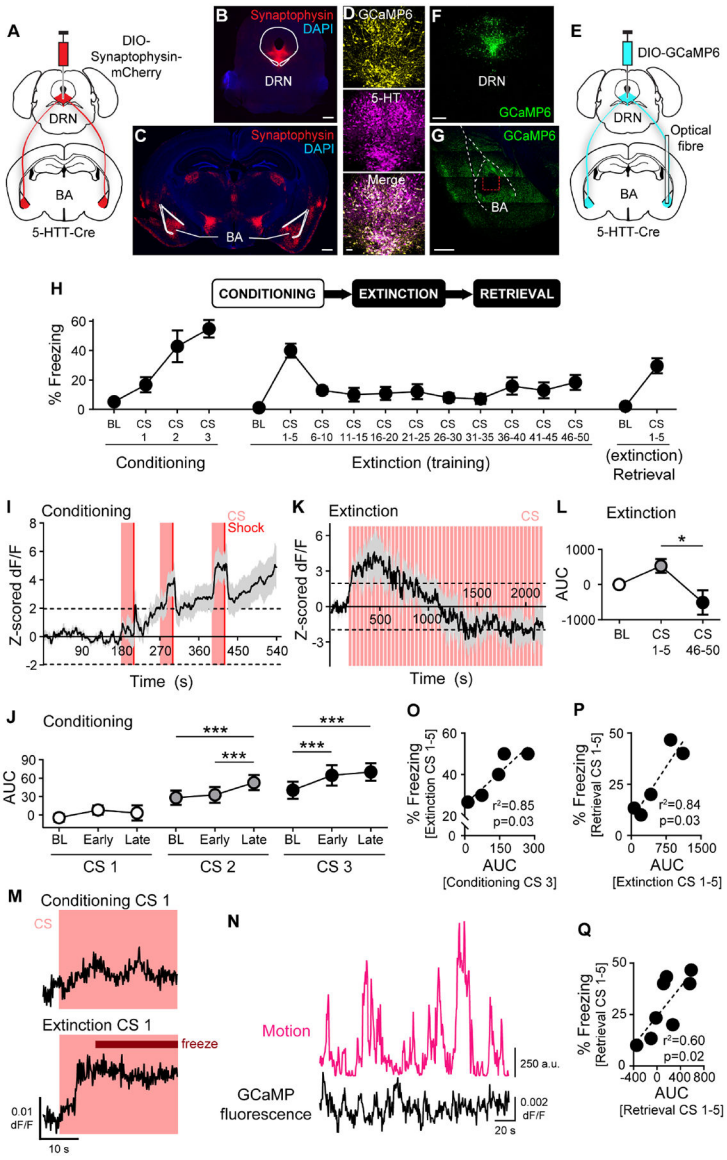

Figure 1. DRN→BA 5-HT pathway activity tracks fear acquisition, expression, and extinction

(A-C) Cre-dependent fluorescent synaptophysin injection into DRN of 5-HTT-Cre mice (A). Fluorescent synaptophysin expression in DRN (B). Scale bar=500 μm. Fluorescent synaptophysin expression in DRN 5-HT projections in BA (C). Scale bar=500 μm.

(D-G) Overlap of GCaMP6(m) expression and 5-HT immunoreactivity in DRN (D). Scale bar=50 μm. Cre-dependent GCaMP6 injection into DRN and unilateral optical fibre implantation into BA of 5-HTT-Cre mice (E). GCaMP6 expression in DRN (F). Scale bar=500 μm. GCaMP6 expression in DRN 5-HT projections in BA (G). Dashed red lines=optical fibre tract. Scale bar=500 μm.

(H) *Top*: Behavioural task. *Bottom*: Freezing in DRN GCaMP6-injected and BA optical fibre-implanted 5-HTT-Cre mice (n=8 mice).

(I and K) DRN→BA 5-HT pathway activity increased during FC (n=7 mice) (I) and temporarily rose during FE (n=5 mice) (K). Traces show mean±SEM of z-scored dF/F

GCaMP fluorescence. Dashed lines at ±1.96 demarcate statistically significant change from baseline (2-tailed, α=0.05).

(J and L) DRN→BA 5-HT activity increased during FC CSs (n=7 mice) (J) and decreased during FE (n=5 mice) (L). Data are mean±SEM of AUC of activity traces from (I) and (K).

(M) Representative traces showing a rise in DRN→BA 5-HT activity preceding a freezing event early in FE, but not during the lack of freezing early in FC. Traces show dF/F GCaMP fluorescence.

(N) Representative traces showing changes in motion (magenta) and dF/F GCaMP fluorescence (black) during pre-FC baseline.

(O-Q) DRN→BA 5-HT pathway activity during FC correlated with freezing behaviour during FE (n=5 mice) (O). DRN→BA 5-HT pathway activity during FE correlated with freezing behaviour during ER (n=5 mice) (P). DRN→BA 5-HT pathway activity correlated with freezing behaviour during ER (n=8 mice) (Q).

AUC—area under the curve, BL—baseline.

*p<0.05, ***p<0.001.

See also Figures S1, S2.

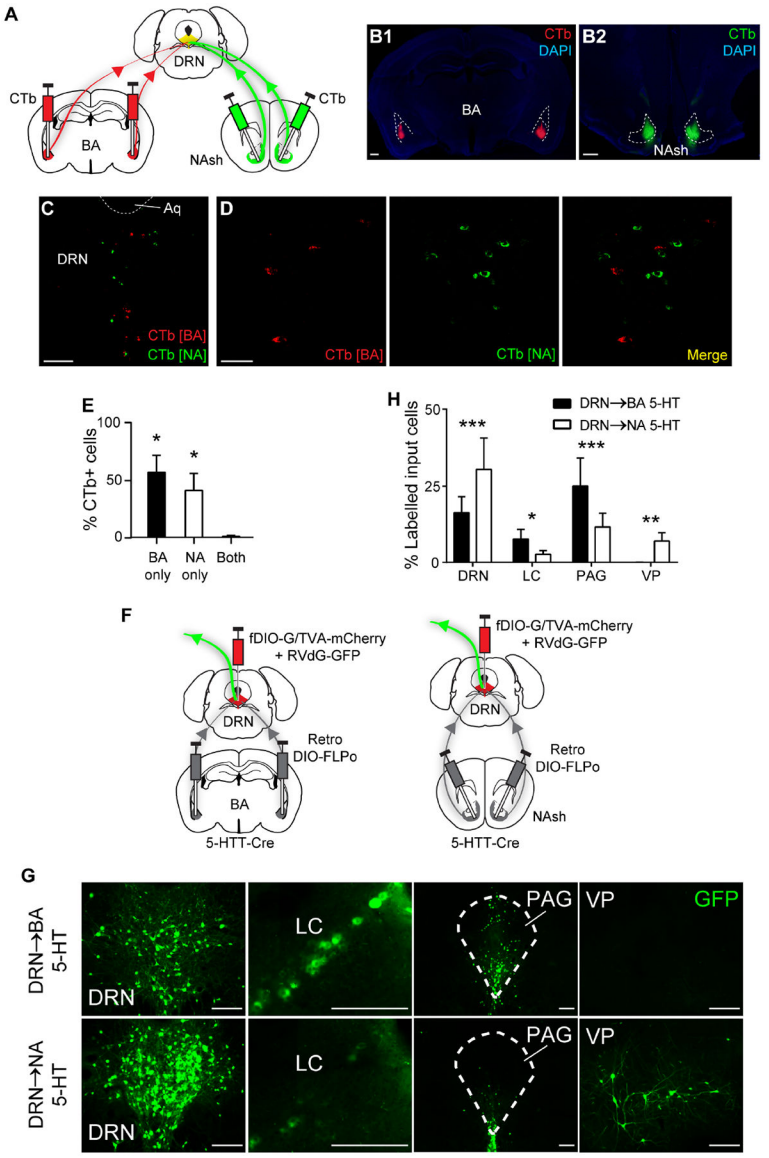

Figure 2. DRN→BA and DRN→NA 5-HT pathways are anatomically distinct

(A–C) Bilateral CTb injections into BA and NA (A). CTb in BA (B1) and NA (B2). Scale bars=500 μm. Dual CTb-labelled cells in DRN (C). Scale bar=250 μm.

(D) Overlay of dual CTb-labelled cells in DRN. Scale bar=40 μm.

(E) Most BA- and NA-projecting DRN neurons were distinct (BA and NA n=5 mice). Data are mean±SEM. *p<0.05 compared to theoretical zero.

(F) Bilateral retro Cre-dependent FLPo injection into BA (*left*) or NA (*right*) and FLPo-dependent rabies GFP injection into DRN of 5-HTT-Cre mice.

(G) GFP+ neurons that input onto DRN 5-HT projections to BA and NA. Scale bars=200 μm.

(H) Differing percentages of input cells to BA- and NA-projecting DRN 5-HT neurons (BA n=5 mice, NA n=5 mice). *See also* Table S1 *for complete distribution of identified input cells*. Data are mean±SEM.

Aq—aqueduct, LC—locus coeruleus, NAsh—nucleus accumbens shell, PAG—periaqueductal grey, VP—ventral pallidum.

*p<0.05, **p<0.01, ***p<0.001.

See also Figure S3, Table S1.

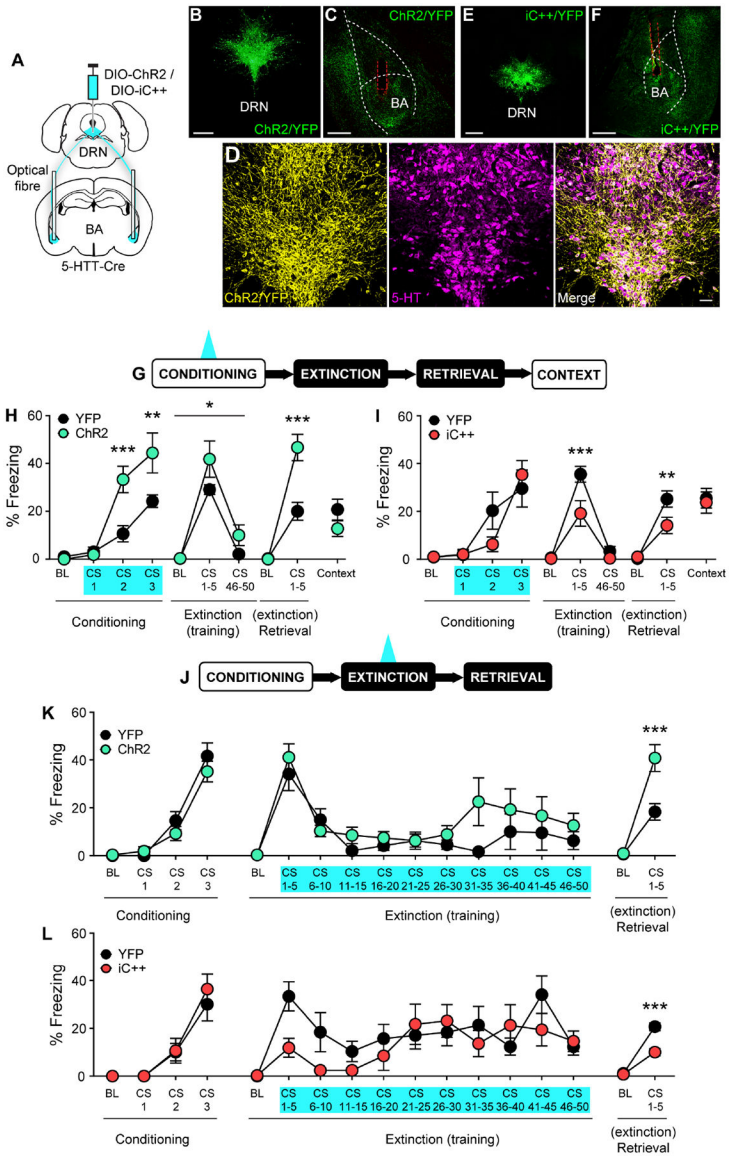

Figure 3. DRN→BA 5-HT pathway bidirectionally regulates fear and extinction learning.

(A-F) Cre-dependent opsin injection into DRN and bilateral optical fibre implantation into BA of 5-HTT-Cre mice (A). ChR2 expression in DRN (B) and in DRN 5-HT projections in BA (C). Scale bars=500 μm. Overlap of ChR2 expression and 5-HT immunoreactivity in DRN (D). Scale bar=50 μm. iC++ expression in DRN (E) and DRN 5-HT projections in BA. (F). Scale bars=500 μm. Dashed red lines=optical fibre tract.

(G-I) Behavioural task. 20 Hz (ChR2) or continuous (iC++) laser stimulation was delivered during FC CSs (G). ChR2 mice froze more than YFP controls during FC, FE, and ER (YFP n=11 mice, ChR2 n=9 mice) (H). iC++ mice froze less than YFP controls during FE and ER (YFP n=9 mice, iC++ n=8 mice) (I). Data are mean±SEM.

(J-L) Behavioural task. 20 Hz (ChR2) or continuous (iC++) laser stimulation was delivered during FE CSs (J). ChR2 mice froze more than YFP controls during ER (YFP n=8 mice,

ChR2 n=9 mice) (K). iC++ mice froze less than YFP controls during ER (YFP n=10 mice, iC++ n=11 mice) (L). Data are mean±SEM.

BL—baseline.

*p<0.05, **p<0.01, ***p<0.001.

See also Figures S3, S4, S5.

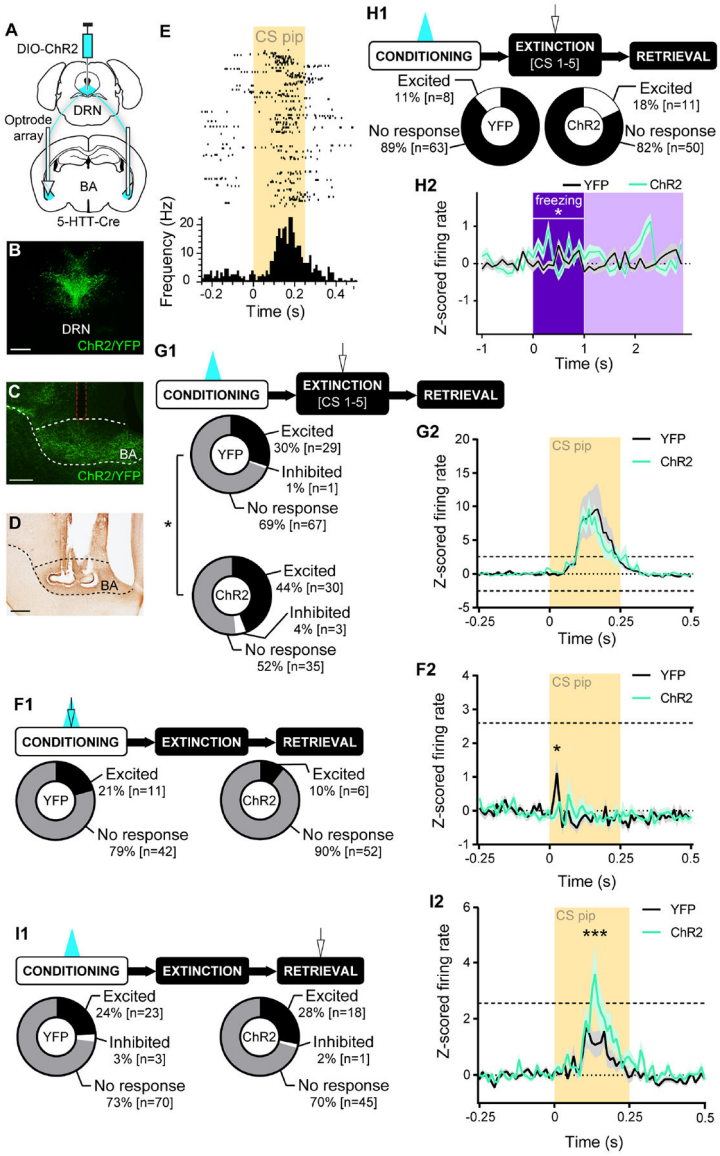

Figure 4. DRN→BA 5-HT pathway sculpts BA neuronal fear encoding

(A-D) Cre-dependent ChR2 injection into DRN and unilateral optrode array implantation into BA of 5-HTT-Cre mice (A). ChR2 expression in DRN (B). ChR2 expression in DRN 5-HT projections in BA (sagittal); dashed red lines=optical fibre tract (C). Bright field image of optrode array placement in BA (sagittal) (D). Scale bars=500 μm.

(E) Raster plot of a BA single unit firing during CS pips in early FE.

(F1) *Top*: Behavioural task. 20 Hz laser stimulation was delivered during FC CSs. *In vivo* electrophysiology data from FC. *Bottom*: No difference in proportion of BA single unit responses to CS pips (YFP n=53 units, 9 mice; ChR2 n=58 units, 9 mice).

(F2) Firing rates of BA single units were lower in ChR2 vs. YFP mice during CS pips (YFP n=53 units, 9 mice; ChR2 n=58 units, 9 mice). Traces show mean±SEM of z-scored firing rate. Dashed lines at +2.58 demarcate statistically significant change from baseline (2-tailed, α=0.01).

(G1) *Top*: Behavioural task. 20 Hz laser stimulation was delivered during FC CSs. *In vivo* electrophysiology data from early FE (CS1–5). *Bottom*: A greater proportion of BA single units was excited during CS pips in ChR2 vs. YFP mice (YFP n=97 units, 9 mice; ChR2 n=68 units, 8 mice).
(G2) Firing rates of BA single units in ChR2 and YFP mice increased during CS pips (YFP n=97 units, 9 mice; ChR2 n=68 units, 8 mice). Traces show mean±SEM of z-scored firing rate. Dashed lines at ±2.58 demarcate statistically significant change from baseline (2-tailed, α=0.01).
(H1) *Top*: Behavioural task. 20 Hz laser stimulation was delivered during FC CSs. *In vivo* electrophysiology data is from early FE (CS1–5). *Bottom*: No difference in proportion of BA single unit firing during freezing onset (YFP n=71 units, 9 mice; ChR2 n=61 units, 8 mice).
(H2) Firing rates of BA single units were higher overall in ChR2 vs. YFP mice during freezing onset (YFP n=71 units, 9 mice; ChR2 n=61 units, 8 mice). Traces show mean±SEM of z-scored firing rate. ±1.96 represents statistically significant change from baseline (2-tailed, α=0.05).
(I1) *Top*: Behavioural task. 20 Hz laser stimulation was delivered during FC CSs. *In vivo* electrophysiology data from ER. *Bottom*: No difference in proportion of BA single unit responses to CS pips (YFP n=96 units, 9 mice; ChR2 n=64 units, 9 mice).
(I2) Firing rates of BA single units were higher in ChR2 vs. YFP mice during CS pips (YFP n=96 units, 9 mice; ChR2 n=64 units, 9 mice). Traces show mean±SEM of z-scored firing rate. Dashed lines at +2.58 demarcate statistically significant change from baseline (2-tailed, α=0.01).
*p<0.05, ***p<0.001.
See also Figures S3 and S6.

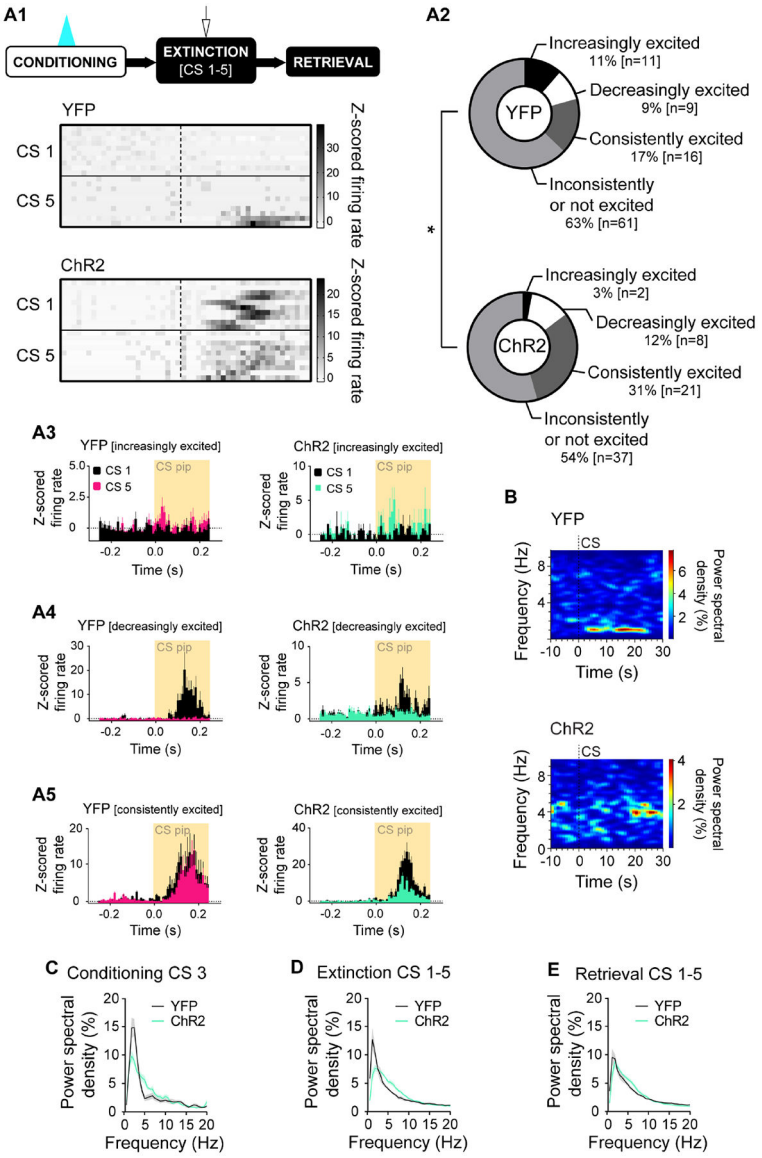

Figure 5. DRN→BA 5-HT pathway alters BA neuronal fear encoding dynamics

(A1) *Top*: Behavioural task. 20 Hz laser stimulation was delivered during FC CSs. *In vivo* electrophysiology data from early FE (CS1–5). *Bottom*: Colour plot showing increasingly excited BA single units in YFP vs. consistently excited BA single units in ChR2 mice during CS pips over the course of CSs. Rows are individual single units.

(A2) A smaller proportion of BA single units became increasingly excited and a larger proportion remained consistently excited in ChR2 vs. YFP mice over the course of CSs (YFP n=97 units, 9 mice; ChR2 n=68 units, 8 mice).

(A3) Increasingly excited BA single units whose firing did not change during CS1 but increased by CS5. ±1.96 represents statistically significant change from baseline (2-tailed, α=0.05). Histograms show mean±SEM of z-scored firing rate.

(A4) Decreasingly excited BA single units whose firing increased during CS1 but no longer changed by CS5. ±1.96 represents statistically significant change from baseline (2-tailed, α=0.05). Histograms show mean±SEM of z-scored firing rate.
(A5) Consistently excited BA single units whose firing increased during CS1 and still increased by CS5. ±1.96 represents statistically significant change from baseline (2-tailed, α=0.05). Histograms show mean±SEM of z-scored firing rate. (B) BA LFPs during FE CSs. (C-E) Power spectral densities of BA LFPs during CSs (FC, YFP n=9 mice, ChR2 n=9 mice; FE, YFP n=9 mice, ChR2 n=8 mice; ER, YFP n=9 mice, ChR2 n=9 mice). Data are mean±SEM.
*$p<0.05$.
See also Figures S3, S6, S7.

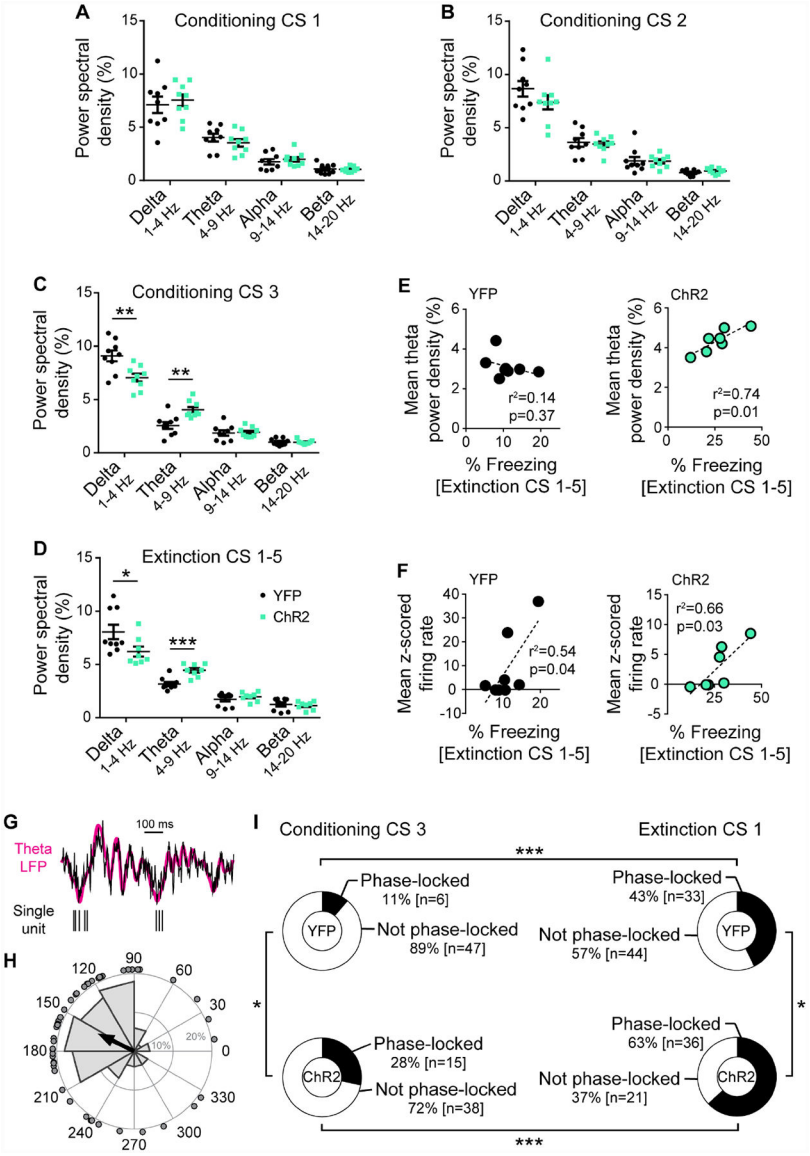

Figure 6. DRN→BA 5-HT pathway accentuates fear-related BA theta power

(A-D) Power spectral densities of BA LFPs in delta, theta, alpha, and beta oscillation ranges at FC CS1–3 (A-C) (YFP n=9 mice, ChR2 n=9 mice) and FE CS1–5 (D) (YFP n=9 mice, ChR2 n=8 mice). Data are mean±SEM.

(E-F) Theta power of BA LFPs (E) and z-scored firing rates of BA single units (F) correlated against freezing behaviour during FE in ChR2 and YFP mice (YFP theta n=9 mice, ChR2 theta n=8 mice, YFP units n=9 mice, ChR2 units n=8 mice).

(G) Representative raw (black) and theta filtered (magenta) BA LFP trace (*top*), and simultaneously recorded BA single unit action potentials (*bottom*) during a CS.

(H) Distribution (grey bars) and mean (black arrow) of theta phases of a BA single unit's action potentials during a CS. Dots depict individual action potentials.

(I) A greater proportion of BA single units were phase-locked to theta during FE vs. FC CSs, and in ChR2 vs. YFP mice (FC YFP n=53 units, 9 mice; FC ChR2 n=53 units, 9 mice; FE YFP n=77 units, 9 mice; FE ChR2 n=57 units, 8 mice).
*p<0.05, **p<0.01, ***p<0.001.
See also Figures S3, S6, S7.

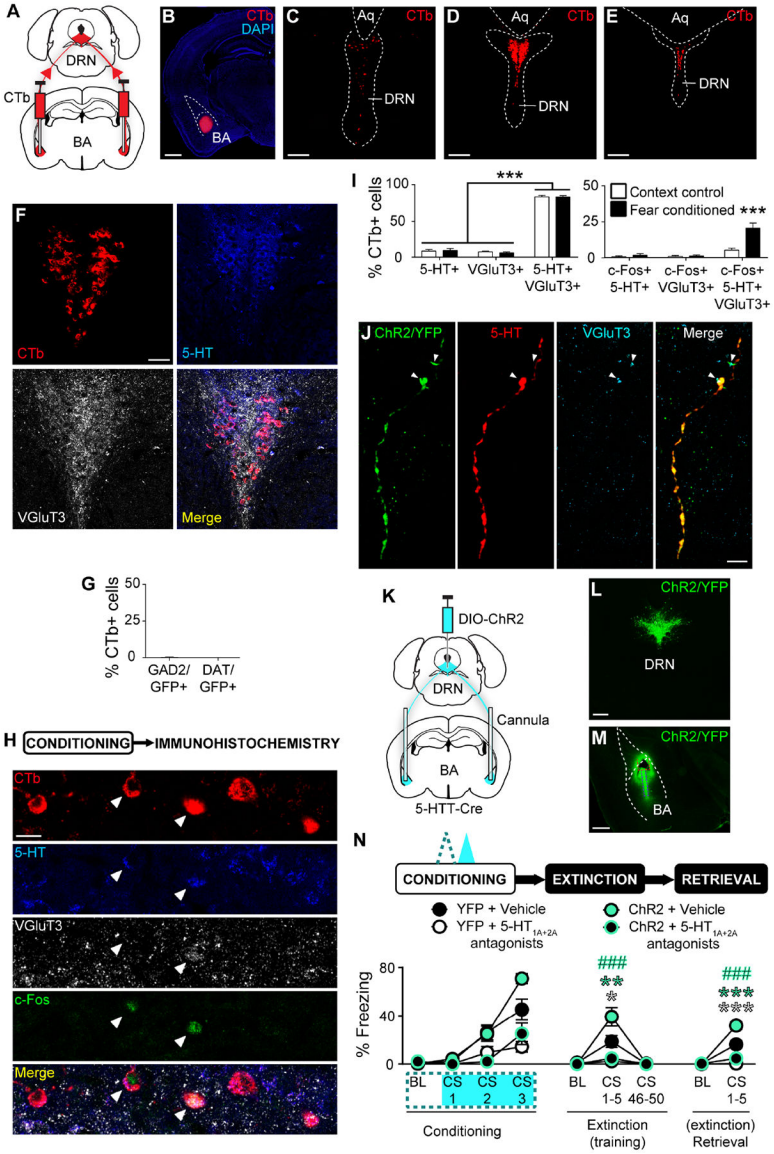

Figure 7. DRN→BA 5-HT neurons co-express VGluT3 but regulate fear via BA 5-HT-R.

(A-E) Bilateral CTb injections into BA (A). CTb in BA (B). Scale bar=1 mm. CTb-labelled cells in rostral (C), middle (D), and caudal (E) DRN. Scale bars=150 μm.

(F) Overlay of CTb+, 5-HT+, and VGluT3+ cells in DRN. Scale bar=50 μm.

(G) Almost no CTb+ DRN neurons expressed GAD2 or DAT (GAD2 n=6 mice, DAT n=5 mice). Data are mean±SEM.

(H) Overlay (single optical section, 1 μm thickness) of CTb+, 5-HT+, VGluT3+, and c-Fos+ cells in DRN post-FC. Scale bar=20 μm.

(I) *Left*: Majority of CTb+ DRN neurons contained 5-HT and VGluT3. *Right*: 5-HT and VGluT3 co-expressing CTb+ DRN neurons were preferentially activated during FC (context control n=6 mice, fear conditioned n=6 mice). Data are mean±SEM.

(J) Overlap of ChR2 expression and immunoreactivity for 5-HT and VGluT3 in axons in BA. VGluT3 (white arrows) and 5-HT appear at slightly different parts of ChR2+ axons. Scale bar=10 μm.

(K-M) Cre-dependent ChR2 injection into DRN and bilateral opto-fluid cannula or optical fibre implantation into BA of 5-HTT-Cre mice (K). ChR2 expression in DRN (L) and DRN 5-HT projections in BA (M). Dashed red lines=cannula tract, dashed purple lines=infusion needle tract. Scale bars=500 μm.

(N) *Top*: Behavioural task. A cocktail of 5-HT_{1A} (WAY100635, 0.37 nmol) and 5-HT_{2A} (MDL100907, 0.54 nmol) antagonists was infused into BA prior to FC. 20 Hz laser stimulation was delivered during FC CSs. *Bottom*: 5-HT-R antagonism prevented increased freezing in ChR2 vs. YFP mice during FE and ER (YFP+VEH n=7 mice; YFP+drug n=7 mice, ChR2+VEH n=8 mice, ChR2+drug n=8 mice). Data are mean±SEM. *p<0.05, **p<0.01, ***p<0.001 compared to YFP+VEH mice; ###p<0.001 compared to. ChR2+VEH mice.

See also Figure S7.

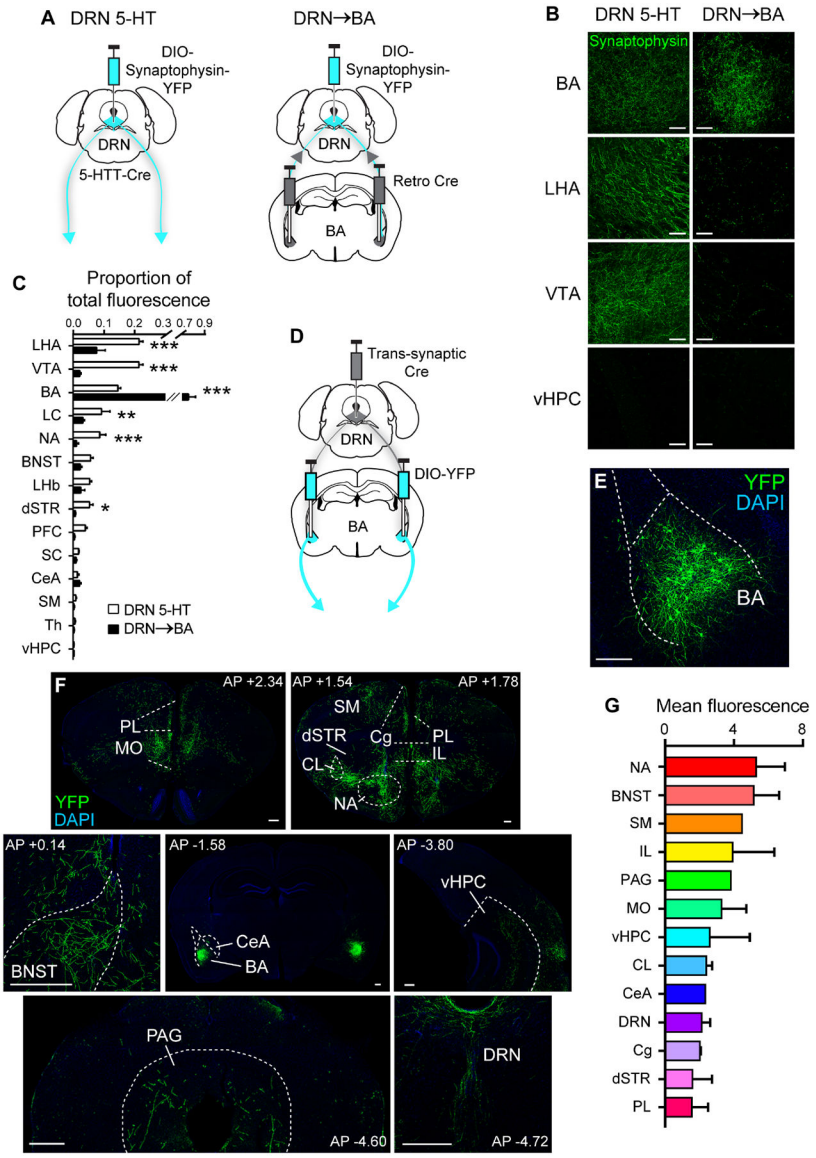

Figure 8. DRN→BA 5-HT pathway is positioned within a broader fear-mediating network

(A) *Left*: Cre-dependent fluorescent synaptophysin injection into DRN of 5-HTT-Cre mice. *Right*: Bilateral retro Cre injection into BA and Cre-dependent fluorescent synaptophysin injection into DRN.

(B) Fluorescent synaptophysin-expressing DRN projections (maximum intensity projections; z-stack: 10 μm, 1 μm optical sections). Scale bars=50 μm.

(C) Proportion of total fluorescence from fluorescent synaptophysin-expressing DRN projections (DRN 5-HT n=3 mice, DRN→BA n=3 mice). Data are mean±SEM.

(D-E) Trans-synaptic Cre injection into DRN and bilateral Cre-dependent YFP injection into BA (D). YFP expression in BA neurons (E). Scale bar=250 μm.

(F) YFP+ BA projections. Scale bars=250 μm.

(G) Fluorescence from YFP+ BA projections (n=4 mice). Data are mean±SEM. BNST—bed nucleus of the stria terminalis, CeA—central amygdala, Cg—cingulate cortex, CL—

claustrum, dSTR—dorsal striatum, IL—infralimbic cortex, LC—locus coeruleus, LHA—lateral hypothalamus, LHb—lateral habenula, MO—medial orbitofrontal cortex, PAG—periaqueductal grey, PFC—prefrontal cortex, PL—prelimbic cortex, SC—superior colliculus, SM—sensory/motor cortices, Th—thalamus, vHPC—ventral hippocampus, VTA—ventral tegmental area.

*p<0.05, **p<0.01, ***p<0.001.

See also Figure S8.

KEY RESOURCES TABLE

REAGENT or RESOURCE	SOURCE	IDENTIFIER	RRID
Antibodies			
Chicken anti-GFP	Abcam	13970	AB_300798
Rabbit anti-DsRed	Clontech	632496	AB_10013483
Goat anti-chicken Alexa 488	Abcam	150169	AB_2636803
Goat anti-rabbit Alexa 555	Life Technologies	A21428	AB_141784
Rabbit anti-c-Fos	Cell Signaling Technology	#2250	AB_2247211
Goat anti-5-HT	Immunostar	20079	AB_572262
Guinea pig anti-VGluT3	Frontier Institute	VGluT3-GP-Af300	AB_2571855
Donkey anti-rabbit Alexa 488	Life Technologies	A21206	AB_141708
Donkey anti-goat Alexa 350	Life Technologies	A21081	AB_141521
Donkey anti-guinea pig Alexa 647	Millipore	AP193SA6	AB_2629452
Rabbit anti-DBH	Immunostar	#22806	AB_572229
Goat anti-rabbit Alexa 488	Life Technologies	A11034	AB_2576217
Bacterial and Virus Strains			
AAVdj-EF1a-DIO-GCaMP6m	Stanford University Neuroscience Gene Vector and Virus Core	GVVC-AAV-92	
AAV2-EF1a-DIO-EYFP	University of North Carolina Vector Core	N/A	
AAV2-EF1a-DIO-hChR2(E123T/T159C)-EYFP	University of North Carolina Vector Core	N/A	
AAV2-EF1a-DIO-iC++-EYFP	University of North Carolina Vector Core	N/A	
AAV8.2-hEF1a-DIO-synaptophysin-eYFP	Gene Delivery Technology Core, Massachusetts General Hospital	N/A	
AAV8.2-hEF1a-DIO-synaptophysin-mCherry	Gene Delivery Technology Core, Massachusetts General Hospital	N/A	
retro-AAV2-Ef1a-Cre	Salk Institute Viral Vector Core	N/A	
retro-AAV2-pEF1a-DIO-FLPo-WPRE-hGHpA	Addgene; Vigene	Addgene cat. # 87306	Addgene_87306
AAV2-FLEx(FRT)-G	Addgene; Vigene	Addgene cat. # 67828	Addgene_67828
AAV2-FLEx(FRT)-TC	Addgene; Vigene	Addgene cat. # 67827	Addgene_67827
EnvA+RVdG-eGFP	Salk Institute Viral Vector Core	N/A	
AAV1-hSyn-Cre-WPRE-hGH	University of Pennsylvania Vector Core	N/A	
Chemicals, Peptides, and Recombinant Proteins			

REAGENT or RESOURCE	SOURCE	IDENTIFIER	RRID
Cholera toxin subunit B (recombinant), Alexa 555	Invitrogen	C34776	
Cholera toxin subunit B (recombinant), Alexa 488	Invitrogen	C22841	
WAY100635 maleate	Tocris Bioscience	4380	
MDL100907	Tocris Bioscience	4173	
Experimental Models: Organisms/Strains			
Mouse: B6.Cg-Tg(Slc6a4-cre)Et33Gsat	Laboratory of Thomas Kash	MMRRC stock. # 031028-UCD	MMRRC_031028-UCD
Mouse: C57BL/6J	Jackson Laboratory	000664	IMSR_JAX:000664
Mouse: B6;129S4-Gt(ROSA)26Sor<tm9(EGFP/Rpl10a)Amc>/J	Jackson Laboratory	024750	IMSR_JAX:024750
Mouse: Gad2<tm2(cre)Zjh>/J	Laboratory of David Lovinger	JAX stock. # 010802	IMSR_JAX:010802
Mouse: B6.SJL-Slc6a3<tm1.1(cre)Bkmn>/J	Jackson Laboratory	006660	IMSR_JAX:006660
Software and Algorithms			
Video Freeze	Med Associates	https://www.med-associates.com/product/video-fear-conditioning/	
Ethovision	Noldus Information Technology Inc.	https://www.noldus.com/animal-behavior-research/products/ethovision-xt	
CinePlex Behavioral Research System	Plexon	https://plexon.com/products/cineplex-behavioral-research-system/#research-system-technical-specs	
Offline Sorter	Plexon	https://plexon.com/products/offline-sorter/	
NeuroExplorer	Nex Technologies	https://www.neuroexplorer.com/	
MATLAB	Mathworks, Inc.	https://www.mathworks.com/products/matlab.html	
Zen lite	Carl Zeiss Microscopy	https://www.zeiss.com/microscopy/us/products/microscope-software/zen-lite.html	
OlyVIA	Olympus	https://www.olympus-lifescience.com/en/support/downloads/	
FIJI (Image J)	Schindelin et al. (2012)	https://fiji.sc/	
GraphPad Prism	GraphPad Software, Inc.	https://www.graphpad.com/scientific-software/prism/	
Other			
Optical fibre for photometry (400 μm, 0.48 numerical aperture)	Doric Lenses	MFC_400/430–0.48_5mm_MF1.25_FLT	
Optical fibre for optogenetics (200 μm, 0.39 numerical aperture)	Thorlabs	CFMLC12U-20	
Electrode array (8 × 2)	Innovative Neurophysiology	N/A	
Opto-fluid cannula	Doric Lenses	DiOFC-LG_P=6.5_320/430_4.7	